

University of Nevada, Reno

Multipole Excitation of Fullerene Molecules in a Semi-Classical Model

A dissertation submitted in partial fulfillment of the  
requirements for the degree of Doctor of Philosophy in

Physics

by

Krishna Prasad Lamichhane

Dr. Peter Winkler/Dissertation Advisor

December, 2010

Copyright by Krishna Prasad Lamichhane, 2010

All Rights Reserved

THE GRADUATE SCHOOL

UNIVERSITY

OF NEVADA

RENO

We recommend that the dissertation prepared under our supervision

by

Krishna Prasad Lamichhane

entitled

Multipole Excitation of Fullerene Molecules in a Semi-Classical Model

be accepted in partial fulfillment of the requirements for the degree of

DOCTOR OF PHILOSOPHY

Peter Winkler, Ph.D., Advisor

Aaron Covington, Ph.D., Committee Member

Alla Safronova, Ph.D., Committee Member

Andrey Esaulov, Ph.D., Committee Member

David M. Leitner, Ph.D., Graduate School Representative

Marsha H. Read, Ph. D., Associate Dean, Graduate School

December, 2010

## Abstract

The local current approximation (LCA) is introduced and derived from a general variational principle. This approach serves as a semiclassical description of strongly collective excitations in finite fermion systems. Here applied for the first time to study the coupling of surface and volume dipole oscillations in the fullerene  $C_{60}$  molecules. The spectrum obtained for the coupling of the pure translational mode with compressional volume modes in the semiclassical LCA shows close agreement with the experimentally observed spectra. Applying the same approach to the photoionization cross section of  $C_{60}$ , we discuss the results of higher multipole resonances of fullerene molecules. The comparison to data obtained from electron scattering experiments reveals the adequacy of the semi-classical approach as well as the collective nature of several high angular momentum resonances. Similar to the results of the dipole case, the coupling of surface and volume plasmon modes in  $C_{60}$  molecules is seen to shift both peaks slightly towards lower energies. Finally we study a simple mechanical model to describe the response of fullerene molecules to an oscillating electric field. In this model, we treat the  $\pi$  and  $\sigma$  electrons of fullerene molecules as two independent harmonic oscillators with differing mass, electrical charge and restoring force, connected by a weak coupling. A third force couples the harmonic oscillators. We explicitly solve the model's equation of motion under the influence of a driving harmonic electric field and a variable damping term. The power consumption of the coupled system is calculated for a range of driving frequencies and damping terms. For an appropriate choice of parameters, the results of this mechanical model show similarity

to the experimentally determined photo-excitation cross-section of  $C_{60}$  molecules.

## Acknowledgement

From bottom of my heart, I would like to take this an opportunity to express my sincere gratitude to my adviser, Professor Dr. Winkler and I would also like to express my deep appreciation for his tremendous help through encouragement and understanding which has been extremely valuable ground for my Ph.D. His vision, Knowledge and constructive way of thinking have been of great value for me and due to that I am able to complete my Ph.D. Dr. Winkler has always been there for me whenever I need his help and for that I am forever grateful to him. I would like to also express my appreciation to Dr. Matthias Brack in Germany for his constructive suggestions and discussions as well as helping me in my computational work. Also I am very grateful to Prof. Dr. Ronald A. Phaneuf for his kind help on area of experimental data which has been of a tremendous help towards completion of my dissertation. I would like to say special thanks to team of my Graduate Committee members: Dr. Aaron Covington, Dr. Alla Safronova, Dr. Andrey Esaulov and Dr. David Leitner, for their help, suggestions and advices which were valuable resources throughout my Ph.D study. A special thanks to all professors who provided me inspiring lessons which helped reinforced my thirst to learn and study more for my ground of dissertation which were highly valuable. An ultimate appreciation goes to Department of Physics who have aided me with my Ph.D study by providing me a teaching assistantship as well as constructive suggestions. Also importantly, providing me all the facilities I needed to help me build a solid foundation on my dissertation that has greatly helped me to go far as I could in my research. In my life, I am

forever grateful to my family especially my parents who have stuck with me during the time of difficulty where they have lost a lot due to my intensive research and trip abroad as well. Importantly I was inspired to complete my study due to their love, motivation, morality support and understanding of my hurdles in achieving the success. I also owe my loving thanks to my wife and kids. So overall in nutshell, without their encouragement , love and understanding, I would have not been able to finish this work.

# Table of Contents

<b>1 Chapter</b>	<b>1</b>
1.1 Motivations and objectives. . . . .	1
1.2 Organization of the Dissertation . . . . .	5
<b>2 Chapter</b>	<b>6</b>
2.1 Theoretical Background . . . . .	6
2.1.1 Introduction . . . . .	6
2.1.2 Giant Dipole resonance(GDR) . . . . .	7
2.1.3 Other Giant Multipole Resonance . . . . .	10
2.1.4 Thomas Fermi Theory . . . . .	14
2.1.5 Density Functional Theory (DFT) . . . . .	15
2.1.6 The extended Thomas-Fermi model . . . . .	18
2.1.7 General Variational Principle . . . . .	19
2.1.8 General inequalities relating moments . . . . .	23
2.1.9 Equation of Motion Approach (EOM) . . . . .	27
2.1.10 Sum Rules, excitation Operators, and Collective Variables . . . . .	28
2.1.11 Evaluation of sum-rules . . . . .	35
<b>3 Chapter</b>	<b>42</b>
3.1 Coupling of surface and volume plasmons in fullerene molecules . . . . .	42
3.1.1 Introduction . . . . .	42

3.1.2	Electrostatic potential of a uniformly charged spherical shell . . . . .	44
3.1.3	Simple Models for Plasmon Oscillations: . . . . .	45
3.1.4	Spherical Jellium Model . . . . .	47
3.1.5	Local Current Approximation (LCA): . . . . .	48
3.2	Coupling of surface and volume dipole oscillations in fullerene molecules	57
3.3	Energies of higher multipole vibrations of fullerenes in a semi-classical approach . . . . .	67
3.3.1	Introduction . . . . .	67
3.3.2	Theoretical Description . . . . .	71
3.3.3	Results and Discussion . . . . .	72
3.3.4	Giant Monopole Resonances (GMR) . . . . .	73
3.3.5	Giant Quadrupole Resonance (GQR) . . . . .	74
3.3.6	Giant Octupole Resonance (GOR) . . . . .	75
<b>4</b>	<b>Chapter</b>	<b>79</b>
4.1	Summary and Conclusions . . . . .	79
<b>5</b>	<b>Appendices</b>	<b>82</b>
5.1	Appendix A : . . . . .	82
5.1.1	Evaluation of equations (2.10.2) and (2.10.3) . . . . .	82
5.1.2	Local density approximation . . . . .	90
5.2	Appendix B : . . . . .	91
5.2.1	solution of the secular equation . . . . .	91

5.3	Appendix C . . . . .	94
5.3.1	Coupled Oscillator System as a Mechanical Analogy to the Responses of $\pi$ - and $\sigma$ - Electrons. . . . .	94
5.3.2	Introduction . . . . .	95
5.3.3	Theory . . . . .	99
5.3.4	Result and discussion . . . . .	105
<b>6</b>	<b>Presentations and Publications</b>	<b>109</b>

## List of Figures

1	Mass spectrum of carbon clusters produced by laser vaporization of a solid graphite rod in an inert atmosphere. . . . .	3
2	Schematic representation of the giant dipole resonance in atomic nuclei	9
3	(a) Isoscalar monopole and quadrupole modes of excitation.(b) Isovector monopole and quadrupole modes of excitation. . . . .	11
4	Schematic representation of breathing mode. . . . .	12
5	Schematic representation of giant quadrupole resonance. . . . .	13
6	(a) The prolate charge distribution, which results in a positive value of electric quadrupole moment $Q$ . (b) The oblate charge distribution, which results in a negative value of $Q$ . . . . .	35
7	Schematic representation of fullerene molecules shell. . . . .	44
8	Plasmon in a thin metallic films . . . . .	46
9	Movement of plasmon in fullerene molecules . . . . .	47
10	Schematic picture of collective oscillations of electrons (dotted lines) against ions (solid lines) in the spherical jellium model for a metal cluster. (a) pure translational, yielding the Mie surface plasmon (Goldhaber-Teller mode in nuclear physics). (b) compressional dipole mode, leading to a volume plasmon (Steinwedel-Jensen-Migdal mode in nuclei) .	55
11	Comparision of the icosahedron structure of the fullerene molecules to that of a soccer ball. . . . .	57

12	Optic response of $C_{60}$ molecules; experimental photoionization cross section result . . . . .	58
13	Surface and volume plasmon in $C_{60}^+$ molecule . . . . .	59
14	Optic response of $C_{60}$ molecules; TDLDA calculation . . . . .	60
15	Density of electrons in fullerene $C_{60}$ molecule. . . . .	61
16	Photoionization experiments have been performed with $C_{60}^+$ ions [13] and lead to excitation of the giant plasmon resonance. . . . .	63
17	Optic response of $C_{60}$ molecules : LCA calculation . . . . .	64
18	Comparison of optic response of $C_{60}$ molecule. Circles: Experimental photoionization cross section [Scully et al]. Solid lines: TDLDA calculations [Rudel et al]. Dashed lines: present LCA calculation. . .	65
19	Convergence of the sum-rule weighted dipole response of $C_{60}$ molecules in the LCA approximation with respect to the number $M$ of coupled modes with $p, p' = 1, \dots, M$ . . . . .	66
20	Inclusion of volume changing operators $Q_L^p$ with $p \geq 7$ shows the convergence of the sum- rule weighted quadrupole response of $C_{60}$ molecules in the LCA with respect to the number $M$ of coupled modes with $p, p' = 2, \dots, M$ . . . . .	75
21	Response of $C_{60}$ molecules to external stimulation; LCA calculation (Quadrupole mode) . . . . .	76
22	Response of $C_{60}$ molecules to extenal stimulation; LCA calculation (Octupole mode) . . . . .	77

23	Coupled system . . . . .	99
24	The average power lost by damped oscillator . . . . .	107
25	Inelastic electron excitation cross section of fullerene molecules, solid line (theoretical result) and points (experimental result),(used by per- mission of author) . . . . .	108

## List of Tables

1	Physical parameters for the fullerene molecule. . . . .	61
2	The optic dipole response of fullerene molecules according to various theoretical and experimental studies. . . . .	62
3	The LCA multipole response of fullerene molecules . . . . .	78

# 1 Chapter

## 1.1 Motivations and objectives.

The optical resonances of metallic clusters have a long history. Medieval craftsmen knew how to finely divide samples of materials in order to exploit their properties with stunning effects. For example, the brilliant colors in medieval stained glass windows in churches result from the resonant light scattering from finely divided gold and silver particles of different size that were judiciously incorporated into the glass. Early photographers also learned that the size of the silver bromide particles deposited onto a glass substrate determined the rate at which they responded to light, forming permanent images. Various metal clusters with electronic interband transitions in the visible range absorb specific colors of light, yielding distinct colors in reflection.

The study of clusters began early in the twentieth century with the pioneering work by Mie [1] on the response of small metal particles to incident light. Despite the insightful and intuitive work of Mie, the cluster science was not recognized as a legitimate field of study until eighty years later, when Knight et al [2], discovered the electronic shell structure in free alkali metal clusters. A new era started with this discovery in which emphasis is put on the quantized motion of the delocalized valence electrons in the mean field created by the ions. Although ionic structure often does not seem to affect very much the properties of alkali and other simple metal clusters, this behavior suggests the jellium model, which is defined by a Hamiltonian that treats the electrons as individual particles but replaces the ionic cores by a uniform positively

charged background. The jellium model is easy to use and rather effective tool for the largest clusters too, but its limitations are hard to exceed and its physical applicability is difficult to judge [3]. Metal clusters today provide a convenient and relatively inexpensive tools to study the properties of finite fermion systems, important building blocks of nanomaterials. Because of their sensitive response, the irradiation of clusters of atoms by light is a highly effective probe of their structure and dynamics [4].

Before 1985, it was generally accepted that elemental carbon exists in two forms: diamond and graphite. But 25 years ago, Kroto and his collaborators identify the signature of new stable form of carbon that consists of clusters of 60 atoms. They called this third allotrope of carbon Buckminster fullerene. In 1990, Physicist D. R. Huffman and his collaborators discovered the way to make bulk quantity of the  $C_{60}$  molecules. The Nobel prize winning discovery of the fullerene  $C_{60}$  molecules in 1985 by Kroto et al and other carbon-cluster molecules with high degrees of symmetry and notable properties prompted a resurgence of interest in clusters of atoms. Kroto et al [5] using laser vaporization technique confirmed the existence of strangely symmetric cluster consisting of sixty carbon atoms. Figure 1 represents the mass spectrum of carbon cluster [6]. Pure carbon is vaporized in an inert atmosphere and vapor condenses into variety of forms including the fullerene. Carbon clusters ranging in size from 2 to nearly 200 atoms have been produced. This spectrum is characterized by three distinct regions: first the small clusters, containing fewer than 25 atoms are detected to have all clusters. Second a new region between 25 and 35 atoms in which few species of any sort were observed. Kroto group called this region the "forbidden

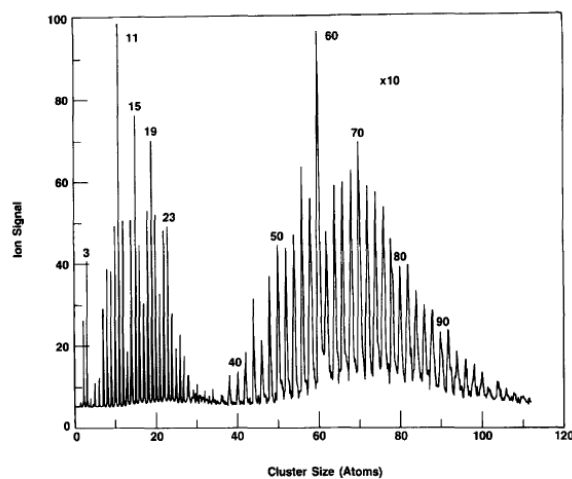


Figure 1: Mass spectrum of carbon clusters produced by laser vaporization of a solid graphite rod in an inert atmosphere.

zone". Third region is an even numbered clusters distribution region extending from the high 30's to well over 150 atoms, including the fullerene  $C_{60}$  molecules.

The carbon atoms assembled on the vertices of a condensed icosahedron with twelve pentagonal and twenty hexagonal faces, formed a structure resembling like a soccer ball. Fullerene molecules sometimes referred to as buckeyballs (named after the American architect, R. Buckminster Fuller, pre-eminent in publicising the geodesic architectural form) with their geodesic structures has been widely described as one of the scientific discoveries of the 20th century. The third form of carbon, a fullerene molecule is an empty, closed cage comprised entirely of  $sp^2$ -hybridized carbon atoms arranged in regular patterns of hexagons and pentagons. Euler's criteria for closed polyhedrons require that every closed fullerene cage structure  $C_n$  consists of 12 pentagons and  $\frac{n}{2} - 10$  hexagons. The fullerene molecule comprised of twelve pentagonal rings is  $C_{20}$ . Thus the fullerene  $C_{20}$  has no hexagons and contains the smallest number

of carbon atoms. There can be any number of hexagons except one. The fullerene  $C_{60}$ , the most accessible but not necessarily the most stable fullerene, contains twelve pentagons and twenty hexagons. The overall number of bonds in a fullerene  $C_n$  is  $\frac{3n}{2}$ . In  $C_{60}$  the length of the bond between two hexagons is  $1.38 \text{ \AA}$ , whereas that between a pentagon and a hexagon is  $1.45 \text{ \AA}$ . At the time of writing and twenty five years since the first pure materials were isolated, over ten thousand scientific papers on fullerenes have been published [7], [8] illustrating the most attractive physical and chemical properties and behaviors of fullerenes and of their growing range of practical applications. The electronic structures of the  $C_{60}$  molecule and its condensed phases has been examined theoretically [9] [10] and experimentally [11]. The crucial interest in Fullerene molecules is due to their unique, highly symmetrical structures which bridge the gap between free molecules and solids. As a result, they demonstrate some of the chemical and physical properties of each area.

A giant resonance due to collective photoexcitation of the 240 delocalized valence electrons of fullerene  $C_{60}$  molecules was predicted by Bertsch and collaborators in 1991 [12]. Soon after their prediction Hertel and collaborators [13] reported the first laboratory measurement of such a giant resonance in free  $C_{60}$  molecules. In this work, we present the "local current approximation" (LCA), approach which includes both the fluid dynamical and sum-rule approaches and can be derived from a variational principle and apply the LCA to collective electronic excitations in  $C_{60}$  molecules, for which the recent experiment [14] have revealed a "volume plasmon", a broad high-energy shoulder in the photo-ionization cross section which can be semiclassically

understood as a compressional component of collective dipole excitation. We discuss the results of higher multipole resonances of fullerene molecules. The comparison to data obtained from electron scattering experiments reveals the adequacy of the semi-classical approach as well as the collective nature of higher angular momentum.

It is also noteworthy to note that the  $C_{60}$  molecule can confine metal atoms such as La, Ca, Ba, Sr etc leading to the differences between the measured properties of free atom and the same atom inside the carbon cage. Puska and Nieminen [60] reported their photoabsorption spectrum of the  $C_{60}$  molecule and those of Xe and Ba atoms placed inside the  $C_{60}$  shell.

## 1.2 Organization of the Dissertation

The organization of this dissertation is as follows. In chapter 2 we present the brief descriptions of the key terms and theory used to proceed with this work. Chapter 3 gives the detailed theory and principal calculations of the work. Two different types of oscillations: dipole oscillation and higher multipole oscillations are closely studied in this chapter. Finally, a summary of this work and conclusions are presented in chapter 4. An appendix A and B contains the steps of calculations and some useful theoretical aspects of collective motion used both in atomic and nuclear physics. An appendix C presents a brief analogy of the fullerene molecule as a system of coupled harmonic oscillators. At the end we listed the presentations and publications in which the author of this dissertation has participated and the references used in this work as well.

## 2 Chapter

### 2.1 Theoretical Background

#### 2.1.1 Introduction

The ab initio calculation of the excited states of fullerene using any of the standard methods of many body theory is a considerable task because of the large number of particles involved and the geometry of the ion lattice. So approximate approaches have been devised to avoid one or both of these difficulties : (a) Replace the exact ion structure by an average positive background potential but treat the valence electrons microscopically. (b) Approximate the ion structures as in part (a) but treat the electrons collectively as a charged oscillating fluid. This dissertation follows the option (b). This has been facilitated by the large body of the work in nuclear physics on collective motion in nuclei which has been modified to serve the present problem. The collective properties of a many-body system are those in which a large number of particles cooperate, in a collective motion, thus losing their individuality. Many authors have presented various methods of studying collective motion in nuclei [15], [16], [17] and [18]. The liquid drop model adopts a semi-classical procedure based on an analogy with a fluid droplet. In this approach two types of collective motion have been studied, one of them are surface vibrations in which the shape is distorted in an oscillatory fashion keeping the volume constant and the other one are volume vibrations, sometimes with preservation of shape. As we know that the nuclear fluid

is nearly incompressible, the lowest excitations are associated with the surface vibrations. For the detail study of low-lying excited states of nuclei, the liquid drop model is inadequate. Very few and too widely spaced levels are predicted by this model [19]. On the other hand, however, we remark that the liquid drop model can easily explain, at least qualitatively, the large quadrupole moments and the strong enhancement of electric dipole transition rates which are conspicuous features of many nuclei and which are hard to fit into a shell theory of the nucleus. It is well known that the optical resonances of  $C_{60}$  can be understood as collective excitations similar to the plasmon resonance in the bulk or the giant resonance in nuclear matter. The local current approximation approach had earlier been successfully applied to study the collective motion in nuclei and clusters. In this work we have applied this LCA approach to the optical response of  $C_{60}$  molecules.

### 2.1.2 Giant Dipole resonance(GDR)

Among the vast variety of possible nuclear excitations, the giant dipole resonance (GDR) is a noticeable example. In the history of nuclear physics two classical models suggested by (a) Goldhaber and Teller [20] and (b) Steinwedel and Jensen [21] describe the physics of the giant dipole resonance (GDR) which was one of the first manifestations of strongly collective excitations in finite fermion systems. In their work, the GDR has been discussed in the framework of a macroscopic model. A Giant resonance occurs when a nucleus is excited by a photon of appropriate energy. As the photon is absorbed by the nucleus protons and neutrons are spatially separated

and polarized. The protons begin to oscillate against the neutrons which try to return the protons to their original positions. The original positions are determined by the fact that a stable nucleus in its ground state has the neutrons and protons distributed in the optimal constellation for the given number of the two species. Any disturbance of this constellation creates a restoring force. Thus oscillation can occur. Getting rid of the excitation energy can occur in various ways. The simplest is by reemission of the photon or by the emission of one or more particles. The latter process is more complicated because it changes the nature of the nucleus but it constitutes usually the preferred decay mode.

The GDR can be observed in most nuclei throughout the periodic table and very little structure is to be seen in the energy dependence of the absorption cross section. The absorption cross section for most nuclei follows a Lorentz curve whose mean energy varies smoothly with mass number. On the basis of a few early experiments Goldhaber and Teller [22] discussed three possible macroscopic explanations for the mass number ( $A$ ) dependence of the resonance energy. They first postulated an elastic binding of the neutrons to the protons that would result in a resonance energy independent of  $A$ . The second proposal, later elaborated by Kohn was that the resonance might consist of density vibrations of the neutron and proton fluids against each other with the surface fixed. This kind of motion, which corresponds to the lowest acoustic mode in a spherical cavity, would result in a resonance energy proportional to  $A^{-\frac{1}{3}}$ . The third suggestion, was that the neutrons and protons might behave like two separate rigid but interpenetrating density distributions. The resulting resonance

consisting of the harmonic displacement of these distributions with respect to each other, would be expected to have an energy dependence proportional to  $A^{-\frac{1}{6}}$ . Figure 2 shows the schematic drawings that illustrates the general feature of the Goldhaber-Teller (GT) and Steinwedel-Jensen (SJ) dipole modes. In the Goldhaber-Teller mode a uniform proton distribution (the smaller sphere whose motion is represented by the solid arrow) vibrates against the neutron sphere. In the Steinwedel-Jensen mode, the neutron simply move back and forth creating the excess of density of neutron (indicated by plus sign) on one side of the nucleus first and then other.

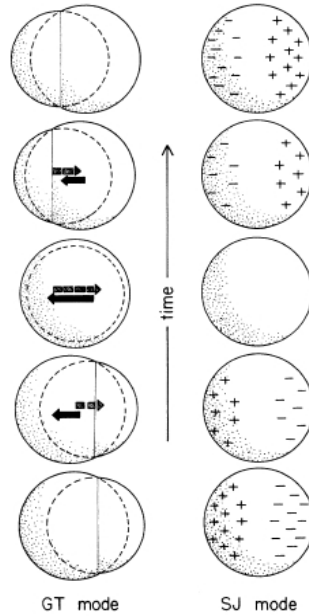


Figure 2: Schematic representation of the giant dipole resonance in atomic nuclei

Goldhaber and Teller interpreted resonances observed in  $(\gamma, n)$  processes at  $\gamma$ -energy 20 MeV as dipole vibrations due to collective motion of all protons relative to all neutrons inside the nucleus. However, Steinwedel and Jensen [21] presented the

more plausible model, of an interpenetrating motion of the proton fluid with density  $\rho_p(\vec{r}, t)$  and neutron fluid with density  $\rho_n(\vec{r}, t)$  under the condition of constant total density  $\rho_0 = \rho_p + \rho_n$  and fixed nuclear radius  $R = R_0 A^{\frac{1}{3}}$ . It was concluded from the detailed analysis of experimental data that a suitable combination of both models is necessary so that the GDR could be classically best understood in terms of coupled translational and compressional dipole modes.

### 2.1.3 Other Giant Multipole Resonance

In the middle of the 20th century the giant resonance field has been extended by observations of number of new resonances. The observation of giant monopole, quadrupole, octopole and other non-dipole resonances has established an entire new subfield in nuclear physics known as giant multipole resonances [23]. In the framework of the liquid drop model one can easily discuss the generalized giant multipole resonances. Figure 3 below shows the quadrupole and monopole modes. If the protons and neutrons are oscillating in phase, the corresponding resonance is called as isoscalar one; if the proton and neutron oscillations are opposite to each other, the mode is denoted as isovector. The isoscalar monopole resonance, the so-called breathing mode, is of special interest because its energy is connected with the compressibility of the nuclear matter [24].

In the giant monopole resonance (GMR) both proton and neutrons move radially in phase leading to an expansion and a contraction of nucleus as shown in figure 4. This is the reason why this vibration is called a breathing mode. This mode does

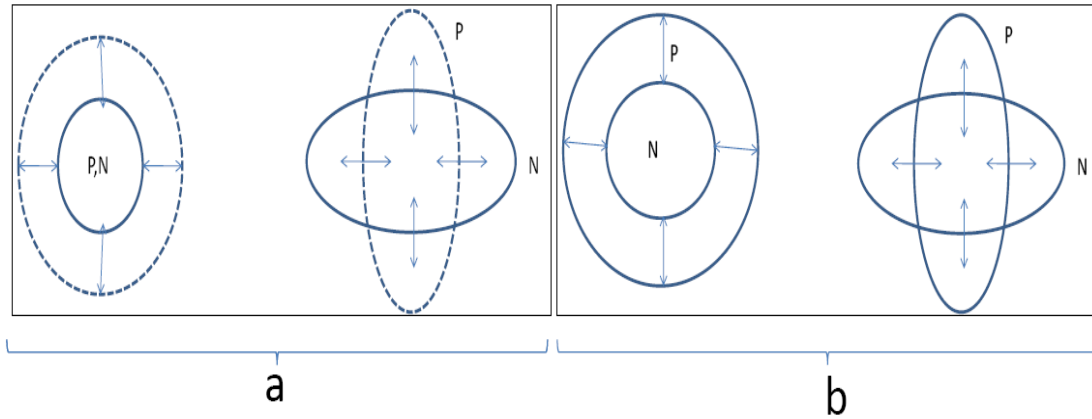


Figure 3: (a) Isoscalar monopole and quadrupole modes of excitation.(b) Isovector monopole and quadrupole modes of excitation.

not couple strongly to photons, but it may be possible to observe it using inelastic electron scattering. The breathing mode for electrons corresponds quite closely to the ordinary plasmon in metals, which is longitudinal sound wave. The energy of the compressional mode will have two components, a coulomb interaction and a modified single-electron kinetic energy [25].

In the giant quadrupole resonance (GQR) the spherical shape is distorted into an ellipsoid and the motion produces alternately elongated and squashed shapes of the nucleus. The physical motion of the particles in the giant quadrupole resonance is shown in figure 5.

Some of these higher multipole resonances have also been predicted and observed in finite electronic systems such as clusters and fullerenes. In the present work, we evaluate sum rules and energies associated with different multipole resonances. In order to describe collective electronic vibrations of multipolarity  $L$ , we shall first use

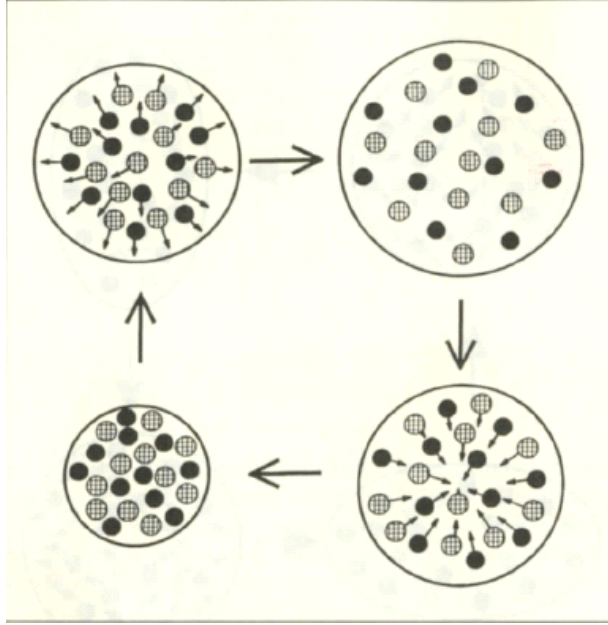


Figure 4: Schematic representation of breathing mode.

the electric multipole operators in the long wavelength limit

$$\hat{Q}_L^p = r^p Y_{L0}(\theta), \quad p = L, L + 1, \dots, N$$

These operators lead to divergence free velocity fields since  $\nabla^2 Q_L^p = 0$ , thus describing pure surface oscillations during which the electron density is translated ( $L = 1$ ) or deformed ( $L > 1$ ) but not compressed. A practical way to compute the excitation energy corresponding to different multipole resonances approximately consists in representing the operator  $Q(\vec{r})$  in terms of a finite set of basis functions  $\{Q_L^p(\vec{r})\}$  :

$$Q(\vec{r}) = \sum_{\lambda=1}^N c_p Q_L^p(\vec{r}) \quad (2.1.1)$$

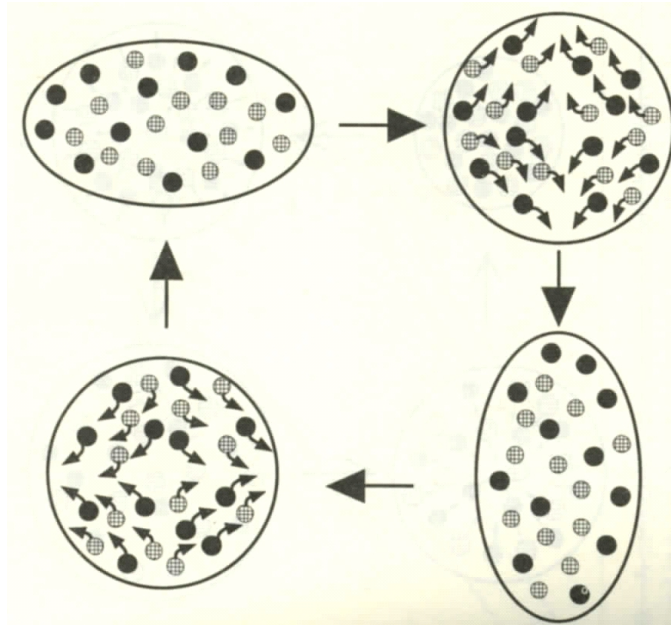


Figure 5: Schematic representation of giant quadrupole resonance.

The first two non dipole multipole operators exciting surface vibrations are quadrupole operator  $Q_2 = r^2 P_2(\cos \theta)$  and the octupole operator  $Q_3 = r^3 P_3(\cos \theta)$ . The monopole operator  $Q_0 = r^2$  effects a breathing mode but not a surface phonon.

To study the different modes of collective excitation of fullerenes  $C_{60}$  and corresponding resonance energy we need to compute the moments (as discussed in section 2.9), whose values, however, clearly depend on the explicit form of the operator  $Q$ . Thus by choosing an efficient approximation to the proper operator one can compute the resonance energy corresponding to the multipole of interest.

### 2.1.4 Thomas Fermi Theory

The Thomas Fermi method is the earliest method which proposed the use of charge density as a fundamental variable instead of the wavefunction. It is the basic form of the density functional theory (DFT) and gives a rough description of the charge density and the corresponding electrostatic potential. The energy as a function of charge density  $\rho(r)$  is written as

$$E_{TF}[\rho(r)] = \int v(r)\rho(r)dr + \int \frac{3}{10} (3\pi^2)^{\frac{2}{3}} \rho^{\frac{5}{3}} dr + \frac{1}{2} \int \frac{\rho(r)\rho(r')}{|r-r'|} dr dr' \quad ((2.4.1))$$

In expression (2.4.1) the third term is coming from the electron -electron interaction and is the electrostatic energy;

$$\therefore E_{es}[\rho] = \frac{1}{2} \int \frac{\rho(r)\rho(r')}{|r-r'|} dr dr' \quad ((2.4.2))$$

with kinetic energy

$$T[\rho] = \int dr t[\rho(r)] \quad ((2.4.3))$$

where  $t[\rho(r)]$  is kinetic energy density for a system of noninteracting electrons with density  $\rho$ . One can get  $t[\rho]$  using the following expression;

$$t[\rho] = 2 \frac{1}{(2\pi)^3} \int_{|k| \leq k_F} dk \frac{\hbar^2 k^2}{2m} \quad ((2.4.4))$$

where

$$\rho = 2 \left( \frac{4\pi}{3} \right) \frac{k_F^3}{(2\pi)^3} \quad ((2.4.5))$$

Again a variational principle is applied and the energy  $E_{TF}[\rho(r)]$  is minimised subject to the condition;

$$\int \rho(r) dr = N \quad ((2.4.6))$$

one gets the well known Thomas-Fermi results. As we know, the T-F theory preceded the DFT and it was an important first step in the wide field of density functional application. However it has a limited accuracy because the kinetic energy functional is only approximate and it does not include the exchange and correlation energy. Thomas-Fermi density variational method has been quite successful at obtaining average energies, densities and other properties of finite fermion systems.

### 2.1.5 Density Functional Theory (DFT)

The basic idea of density-functional theory is almost as old as quantum mechanics and was used by Thomas (1927) and Fermi (1928) in their famous work: to calculate the total energy of a system by an integral over an expression depending only on the local ground-state density  $\rho(r)$ . Most electronic structure calculations these days for solids are based on density functional theory (DFT), originating from the work of Hohenberg, Kohn and Sham [26], [27], [28]. The Hohenberg-Kohn theorem states

that the exact ground-state energy of a correlated electron system is a functional of the density  $\rho(r)$  and that this functional has its variational minimum when evaluated for the exact ground-state density [3]. This approach has become popular for atoms and molecules as well. In density functional theory, the electronic orbitals are the solutions to a Schrödinger equation which depends on the electron density rather than on the individual electron orbitals. Thus this theory replaces the complicated many body wave function  $\Psi(r_1, r_2, \dots, r_N)$  with its corresponding Schrödinger equation by a theoretical approach based on the electron density  $\rho(\vec{r})$  and associated calculational schemes. In order to avoid the difficulty of finding an explicit density functional for kinetic energy, Kohn and Sham proposed to write density in the form of

$$\rho(\vec{r}) = \sum_{i=1}^N |\varphi_i(r)|^2 \quad (2.4.7)$$

in terms of some trial single-particle wave functions  $\varphi_i(r)$ . In principle, this theory includes the exchange and correlation contributions which is not taken into account in Hartree-Fock approach. Practically, however, the exchange and correlation terms are evaluated approximately. The application of density functional theory in different frameworks are collected in references [29], [30], [31], [32], [33]. In DFT the Thomas-Fermi kinetic energy density is proportional to  $\rho^{\frac{5}{3}}$  with constant density. Thus the kinetic energy functional is written as

$$T_{TF}[\rho] = C_F \int \rho^{\frac{5}{3}}(\vec{r}) d\vec{r} \quad (2.4.8)$$

with

$$C_F = \frac{3}{10} (3\pi^2)^{\frac{2}{3}} = 2.871 \text{ in atomic unit.} \quad (2.4.9)$$

Now the total energy functional of the Thomas-Fermi theory of atoms without exchange and correlation terms is given as

$$E_{TF}[\rho(r)] = C_F \int \rho^{\frac{5}{3}}(\vec{r}) d\vec{r} - z \int \frac{\rho(\vec{r})}{r} dr + \frac{1}{2} \int \int \frac{\rho(\vec{r}_1)\rho(\vec{r}_2)}{|\vec{r}_1 - \vec{r}_2|} d\vec{r}_1 d\vec{r}_2 \quad (2.5.1)$$

This expression has to be modified appropriately for the molecules, especially the second term must be modified. Too many modification of the Thomas-Fermi theory have been made after Thomas and Fermi developed their theory in 1920. The total energy functional for the ground state of an atom, for instance, is then minimized with respect to the parameter  $\rho(\vec{r})$ , under the constraint

$$\int \rho(r) dr = N \quad (2.5.2)$$

where  $N$  is the total number of electrons in the atom. As we know that the ground state electron density satisfies the variational principle, we can write

$$\delta \left\{ E_{TF}[\rho(r)] - \mu \left( \int \rho(r) dr - N \right) \right\} = 0 \quad (2.5.3)$$

where  $\mu$  is the Langrange multiplier. Solving for  $\rho(r)$  using equation (2.5.2) and (2.5.3) and substituting  $\rho(r)$  in (2.5.1) we get the total energy  $E$ . In Exact density

functional theory, one can compute the ionization potential for atoms or the work function for bulk metal by using Kohn and Sham equations.

### 2.1.6 The extended Thomas-Fermi model

If the higher order correction terms in  $\hbar$  are added to the Thomas-Fermi model, then this model is called the extended Thomas-Fermi (ETF) model. To apply the ETF method in many fermion system, one needs to include only those terms in the  $\hbar$  expansion that give the finite contribution to the energy. In this model the kinetic energy functional is written as

$$T_{ETF}[\rho] = T_{TF}[\rho] + T_2[\rho] + T_4[\rho] + \dots \quad (2.5.4)$$

where

$$T_{TF}[\rho] \propto \rho^{\frac{5}{3}}$$

is zeroth order kinetic energy term,

$$T_2[\rho] = \frac{\hbar^2}{2m} \left[ \frac{1}{36} \frac{(\nabla\rho)^2}{\rho} + \frac{1}{3} \nabla^2\rho \right] \quad (2.5.5)$$

second order kinetic energy term and

$$T_4[\rho] = \frac{\hbar^2}{2m} \frac{(3\pi^2)^{-\frac{2}{3}}}{6480} \int \rho^{\frac{1}{3}} \left[ 8 \left( \frac{\nabla\rho}{\rho} \right)^4 - 27 \left( \frac{\nabla\rho}{\rho} \right)^2 \frac{\nabla^2\rho}{\rho} + 24 \left( \frac{\nabla^2\rho}{\rho} \right)^2 \right] d^3r \quad (2.5.6)$$

fourth order kinetic energy term [34]. This model is applicable for the slowly

varying densities. For the detailed discussion of the fast and slowly varying densities it better to check the references [3] and [35].

### 2.1.7 General Variational Principle

Another successful approach to evaluate ground and excited state energies is given by the equation of motion method (EOM). It is the method of choice for the present work. Here we start with the equation of motion for a many body system described by a Hamiltonian  $\hat{H}$  with ground state  $|0\rangle$  and energy  $E_0$ . Before writing the equation of motion let us define the creation and annihilation operators of all the eigenstates obey the equation of motion for the excitation operators. If  $|0\rangle$  is the ground state of the system, it is possible to define operators  $\hat{O}_\nu^+, \hat{O}_\nu$  so that  $\hat{O}_\nu^+$  operates on  $|0\rangle$  to create any vibrational state  $|\nu\rangle$  and  $O_\nu$  brings the excited state back to the ground state. For example:

$$\hat{O}_\nu^+ |0\rangle = |\nu\rangle, \quad \hat{O}_\nu |\nu\rangle = |0\rangle$$

are the creation and annihilation operators respectively and

$$\hat{O}_\nu |0\rangle = 0.$$

Now the EOM can be written as

$$\langle 0 | \hat{O}_\nu [\hat{H}, \hat{O}_\nu^+] | 0 \rangle = \hbar\omega_\nu \langle 0 | \hat{O}_\nu \hat{O}_\nu^+ | 0 \rangle \quad (2.6.1)$$

$$\langle 0 | \hat{O}_\nu [\hat{H}, \hat{O}_\nu] | 0 \rangle = \hbar\omega_\nu \langle 0 | \hat{O}_\nu \hat{O}_\nu | 0 \rangle = 0 \quad (2.6.2)$$

Associated with the equation of motion above, the following variational principle can be derived [36]. Solving the equation of motion (2.6.1) and (2.6.2) for the lowest excited state is equivalent to solving the variational equation

$$\frac{\delta E_3 [\hat{Q}]}{\delta \hat{Q}} = 0 \quad (2.6.3)$$

where  $E_3$  is defined by

$$E_3 [\hat{Q}] = \sqrt{\frac{m_3 [\hat{Q}]}{m_1 [\hat{Q}]}}$$

and the moments  $m_1$  and  $m_3$  are defined as the multiple commutators

$$m_1(\hat{Q}) = \frac{1}{2} \langle 0 | [\hat{Q}, [\hat{H}, \hat{Q}]] | 0 \rangle \quad (2.6.4)$$

$$m_3(\hat{Q}) = \frac{1}{2} \langle 0 | [[\hat{H}, \hat{Q}], [\hat{H}, [\hat{Q}, \hat{H}]]] | 0 \rangle \quad (2.6.5)$$

The exact operator  $\hat{Q}$  is not known. It is required to be Hermitean and is generally nonlocal. The values of the moments, however, depend on the explicit form of  $\hat{Q}$ . So we need a convenient set of approximate operators  $Q_L^p(\vec{r})$  from which we can build  $\hat{Q}$  in a variational procedure. These operators will be defined below.

The excitation spectrum can be produced by successive orthogonalization of  $\hat{Q}$ . In the fluid dynamical approach, one approximates the collective excitation energies

$\hbar\omega_\nu$  by the energy  $E_3 [\hat{Q}_\nu]$  with  $\nu$  relating to a particular excitation energy.

The variation  $\delta\hat{Q}$  of an operator can be understood as a variation of the matrix elements of the operator in the matrix mechanics picture. Therefore we can write as usual

$$0 = \frac{\delta}{\delta\hat{Q}} \left( \frac{m_3 [\hat{Q}]}{m_1 [\hat{Q}]} \right)^{\frac{1}{2}} = \frac{1}{2} \left( \frac{m_3 [\hat{Q}]}{m_1 [\hat{Q}]} \right)^{-\frac{1}{2}} \frac{\delta}{\delta\hat{Q}} \left( \frac{m_3 [\hat{Q}]}{m_1 [\hat{Q}]} \right) \quad (2.6.6)$$

and noting that the first factors in the expressions to the right are just  $\frac{1}{2E_3}$ ,

$$0 = \frac{\delta}{\delta\hat{Q}} \left( \frac{m_3 [\hat{Q}]}{m_1 [\hat{Q}]} \right) = \frac{1}{m_1 [\hat{Q}]} \frac{\delta m_3 [\hat{Q}]}{\delta\hat{Q}} - \frac{m_3 [\hat{Q}]}{m_1 [\hat{Q}]^2} \frac{\delta m_1 [\hat{Q}]}{\delta\hat{Q}} \quad (2.6.7)$$

is obtained. With the definition  $E_3 = \hbar\omega_1$  equation (2.6.7) turns into

$$\frac{\delta m_3 [\hat{Q}]}{\delta\hat{Q}} - (\hbar\omega_1)^2 \frac{\delta m_1 [\hat{Q}]}{\delta\hat{Q}} = 0 \quad (2.6.8)$$

The variations

$$\delta m_3 [\hat{Q}] = m_3 [\hat{Q} + \delta\hat{Q}] - m_3 [\hat{Q}]$$

$$\delta m_1 [\hat{Q}] = m_1 [\hat{Q} + \delta\hat{Q}] - m_1 [\hat{Q}]$$

are evaluated by direct application of the commutation rules (2.6.4) and (2.6.5),

leading to

$$\langle 0 | \left[ [\delta\hat{Q}, \hat{H}], \left( [\hat{H}, [H, \hat{Q}]] - (\hbar\omega_1)^2 \hat{Q} \right) \right] | 0 \rangle = 0 \quad (2.6.9)$$

With  $\delta\hat{Q}$  Hermitean,  $[\delta\hat{Q}, \hat{H}]$  is anti-Hermitean, and (2.6.9) therefore is an equation of the form  $c + c^* = 0$  with

$$c = \langle 0 | \left[ [\delta\hat{Q}, \hat{H}], \left( [\hat{H}, [H, \hat{Q}]] - (\hbar\omega_1)^2 \hat{Q} \right) \right] | 0 \rangle \in \mathbb{C} \quad (2.6.10)$$

Since  $|0\rangle$  by definition is the exact ground state of  $H$ , and (2.6.10) must hold for any  $\delta\hat{Q}$  one obtains

$$\left( [\hat{H}, [\hat{H}, \hat{Q}]] - (\hbar\omega_1)^2 \hat{Q} \right) | 0 \rangle = 0 \quad (2.6.11)$$

This resembles the equation of motion for a harmonic oscillator. Therefore  $\hat{Q}$  is interpreted as a generalized coordinate, and in analogy to the well-known algebraic way of solving the harmonic oscillator problem,  $\hat{Q}$  is written as a linear combination

$$\hat{Q} = O_1^+ + O_1 \quad (2.6.12)$$

of the creation and annihilation operator for the first excited state. Inserting (2.6.12) into (2.6.11) one obtains the two equations

$$[\hat{H}, [\hat{H}, O_1^+]] | 0 \rangle = (\hbar\omega_1)^2 O_1^+ | 0 \rangle \quad (2.6.13)$$

$$\left[ \hat{H}, \left[ \hat{H}, O^+ \right] \right] |0\rangle = (\hbar\omega_1)^2 O_1 |0\rangle = 0 \quad (2.6.14)$$

First we consider (2.6.13). After closing with the state  $\langle 1|$ , one exploits that, by definition,  $|0\rangle$  and  $|1\rangle$  are eigenstates of  $H$  and evaluates the outer commutator by letting  $H$  act once to the left and once to the right. One further recalls that  $\langle 1| = \langle 0|O_1$ , and finally obtains

$$\langle 0|O_1 [H, O_1^+] |0\rangle = \hbar\omega_1 \langle 0|O_1 O_1^+ |0\rangle \quad (2.6.15)$$

This is exactly equation (2.6.1) for the first excited state. In the same way, (2.6.2) is obtained from (2.6.14), and the derivation of the general variational principle is finished.

It is possible, in principle to calculate the exact excitation energies and states of the system from the variational principle (2.6.3). But for the practical computations one has to make some ansatz for the operator  $\hat{Q}$ . The exactness of the solution to the true excitations will then depend on how good the ansatz for  $\hat{Q}$  is.

### 2.1.8 General inequalities relating moments

To discuss the electronic multipole vibrations of valence electrons in spherical metal clusters it is essential to relate the different moments  $m_k$  of the strength function  $S(E)$  corresponding to different values of  $k$  through a chain of inequalities obtainable from Schwartz's inequality. The response of the ground state of the system to the

action of an operator  $Q$ , is completely characterized by  $S_Q(E)$ . The  $k$ th moments of  $S_Q(E)$  are defined by

$$m_k(Q) = \int_0^\infty E^k S_Q(E) dE = \sum_{n \neq 0} (E_n)^k |\langle n | Q | \tilde{0} \rangle|^2 \quad ((2.7.1))$$

Where  $|\tilde{0}\rangle$  and  $|n\rangle$  are the correlated ground and excited states of the system, satisfying  $\langle \tilde{0} | \tilde{0} \rangle = \langle n | n \rangle = 1$  and  $E_n$  are the excitation energies. In terms of sum rules the moments  $m_3$  and  $m_1$  can be expressed as the following ground state expectation values[37]

$$m_1(Q) = \frac{1}{2} \langle \tilde{0} | [[Q, [H, Q]] | \tilde{0} \rangle \quad (2.7.2)$$

$$m_3(Q) = \frac{1}{2} \langle \tilde{0} | [[[H, Q], [H, [Q, H]]] | \tilde{0} \rangle \quad (2.7.3)$$

here  $H$  is the total Hamiltonian of the system. According to theorem by Thouless the expression (2.7.2) and (2.7.3) can be evaluated replacing the correlated ground state  $|\tilde{0}\rangle$  by the uncorrelated ground state  $|0\rangle$  on the right hand side of eqs.(2.7.2) and (2.7.3) without introducing any error [38]. Even though we deemphasize the RPA method in the present work, it is important to note that the RPA moments  $m_k$  with other indices  $k$  can in general, not be evaluated from the uncorrelated ground-state wave functions [37]. It has, however, been shown that the negative-energy-weighted sum rule  $m_{-1}$  is related to the static ground-state polarizability  $\alpha_{pol}(Q)$ , which can be evaluated from a constrained HF variational procedure solving  $\delta \langle H - \lambda Q \rangle = 0$

with the Lagrange multiplier  $\lambda$ , by

$$m_{-1}(Q) = \frac{1}{2}\alpha_{pol}(Q) \quad (2.7.4)$$

In this work, we do not start from a HF solution, but ideally, from the solution of the Kohn-Sham equation. The sum rules (2.7.2) and (2.7.3) are evaluated in semiclassical approach and rewritten in terms of functionals of the density  $\rho(r)$ . The validity of the chain of inequalities is founded on the positivity of the strength function  $S(E)$ , i.e  $S(E) > 0$  for all  $E$ , which follows from its definition, one writes then Schwartz's inequality as

$$\int f(E)^2 \rho(E) dE \int g(E)^2 \rho(E) dE \geq (\int f(E) g(E) \rho(E) dE)^2 \quad (2.7.5)$$

where  $\rho(E)$  is a positive definite function,  $\rho(E) dE$  is a positive measure, and  $f$  and  $g$  are arbitrary functions. The strength function  $S(E)$  is defined for positive values of  $E$ , so that

$$\rho(E) = E^k S(E) \quad (2.7.6)$$

is a density function (positive definite and assumed normalizable)[13]. Therefore using expression (2.7.5) with  $\rho(E)$  obtained from (2.7.6) and  $f(E) = E$  and  $g(E) = 1$  we get

$$m_{k+2}m_k \geq m_{k+1}^2 \quad (2.7.7)$$

or

$$\frac{m_{k+2}}{m_{k+1}} \geq \frac{m_{k+1}}{m_k} \quad (2.7.8)$$

and finally by the use of (2.7.8), one can write

$$\dots \geq \frac{m_{k+2}}{m_{k+1}} \geq \sqrt{\frac{m_{k+2}}{m_k}} \geq \frac{m_{k+1}}{m_k} \geq \sqrt{\frac{m_{k+1}}{m_{k-1}}} \geq \dots \quad (2.7.9)$$

The fact that these quantities are homogeneous to an energy, suggests a definition of the energies  $E_3$  and  $E_1$  as

$$E_3 = \sqrt{\frac{m_3}{m_1}}, \quad E_1 = \sqrt{\frac{m_1}{m_{-1}}} \quad (2.7.10)$$

It is thus possible to estimate the position and the width of a RPA mode, whose collective strength is concentrated in one peak, without performing the RPA calculation but simply by calculating the sum rules (2.7.2) and (2.7.3) and the static polarizability (2.7.4). We should deemphasize here the RPA framework. The energies  $E_k$  corresponding to different values of  $k$  will be relevant to different energy domains of collective excitations.

### 2.1.9 Equation of Motion Approach (EOM)

The equation of motion approach has been widely used in studying the collective degrees of freedom in nuclei [46], but it is general enough to be applied to the most many-body systems. So we find a wide spectrum of applications also in theoretical chemistry from early calculations of electron affinities [39] and photodetachment energies [40] of molecules to more recent and more comprehensive representations of theories of general electronic excitations [41] to [44].

The basic idea of the equation of motion approach is to evaluate relationships among the observables corresponding to the excitation operators of the system of interest rather than calculating the wave functions, thereby optimizing our efforts to obtain the best possible values for the observables. Let us consider a many body system described by a Hamiltonian  $H$  with a ground state  $|0\rangle$  of energy  $E_0$ . Suppose  $|\nu\rangle, \nu \neq 0$ , are the excited states and  $E_0 + \hbar\omega_\nu$  the energies of the system. In principle these can be obtained exactly as the solution of the equation of motion [45]

$$\langle 0 | \hat{O}_\nu [H, \hat{O}_\nu^+] | 0 \rangle = \hbar\omega_\nu \langle 0 | \hat{O}_\nu \hat{O}_\nu^+ | 0 \rangle \quad (2.8.1)$$

$$\langle 0 | \hat{O}_\nu [H, \hat{O}_\nu] | 0 \rangle = \hbar\omega_\nu \langle 0 | \hat{O}_\nu \hat{O}_\nu | 0 \rangle = 0 \quad (2.8.2)$$

where the operators  $\hat{O}_\nu, \hat{O}_\nu^+$  are defined as the annihilation and creation operators of the excited states of the system:

$$\hat{O}_\nu^+ |0\rangle = |\nu\rangle, \quad \hat{O}_\nu |\nu\rangle = |0\rangle \quad \text{and} \quad \hat{O}_\nu |0\rangle = 0$$

The exact solutions of the equation (2.8.1) and (2.8.2) are unknown for most systems. A variety of methods for the computation of approximations to the true excited states have been derived, for example, the Hartree-Fock (HF) approximation, the Hartree-Bogolyubov (HB) approximation, the Tamm-Dancoff approximation and the random phase approximation (RPA) [46].

### 2.1.10 Sum Rules, excitation Operators, and Collective Variables

Sum-rules provide useful yardsticks for measuring quantitatively the degree of collectiveness of a given excited state. The best known sum rule is the Thomas-Reiche-Kuhn (TRK) sum rule

$$\sum_{\nu} (E_{\nu} - E_0) \left| \langle 0 | \hat{Q} | \nu \rangle \right|^2 = \frac{3\hbar^2}{2m} \quad (2.9.1)$$

where  $|\nu\rangle$  and  $E_{\nu}$  are eigenstates of the Hamiltonian and the corresponding eigenvalue.  $|0\rangle$  and  $E_0$  are the ground state and the corresponding energy [47]. For a general excitation operator  $\hat{Q}$  one we find

$$\begin{aligned} \sum_{\nu} (E_{\nu} - E_0) \left| \langle 0 | \hat{Q} | \nu \rangle \right|^2 &= \sum_{\nu} (E_{\nu} - E_0) \langle 0 | \hat{Q} | \nu \rangle \langle 0 | \hat{Q} | \nu \rangle^* \\ &= \sum_{\nu} (E_{\nu} - E_0) \langle 0 | \hat{Q} | \nu \rangle \langle \nu | \hat{Q}^{\dagger} | 0 \rangle \\ &= \sum_{\nu} \langle 0 | [\hat{Q}, H] | \nu \rangle \langle \nu | \hat{Q}^{\dagger} | 0 \rangle \end{aligned}$$

$$\sum_{\nu} (E_{\nu} - E_0) \left| \langle 0 | \hat{Q} | \nu \rangle \right|^2 = \langle 0 | [\hat{Q}, H] \hat{Q}^{\dagger} | 0 \rangle \quad (2.9.2)$$

If  $\hat{Q}$  is a Hermitean operator, the summation can also be written as

$$\begin{aligned} \sum_{\nu} (E_{\nu} - E_0) \left| \langle 0 | \hat{Q} | \nu \rangle \right|^2 &= \sum_{\nu} (E_{\nu} - E_0) \langle 0 | \hat{Q} | \nu \rangle \langle \nu | \hat{Q} | 0 \rangle \\ &= - \sum_{\nu} \langle 0 | \hat{Q} | \nu \rangle \langle \nu | [\hat{Q}, H] | 0 \rangle \\ &= - \langle 0 | \hat{Q}, [\hat{Q}, H] | 0 \rangle \end{aligned} \quad (2.9.3)$$

Combine equation (2.9.2) and (2.9.3) we have the following sum rule for a Hermitean operator

$$\sum_{\nu} (E_{\nu} - E_0) \left| \langle 0 | \hat{Q} | \nu \rangle \right|^2 = \frac{1}{2} \langle 0 | [\hat{Q}, [\hat{Q}, H]] | 0 \rangle$$

To quantify the response of many body systems to an excitation operator  $\hat{Q}$  one defines the associated strength function  $S_Q(E)$  as

$$S_Q(E) = \sum_{\nu > 1} \left| \langle \nu | \hat{Q} | 0 \rangle \right|^2 \delta(E - E_{\nu}) \quad (2.9.4)$$

where  $E_{\nu}$ ,  $|\nu\rangle$  are the exact eigensolutions of the total Hamiltonian. The energy-weighted moments  $m_k$  of  $S_Q(E)$  are defined as

$$m_k(Q) \equiv \int_0^{\infty} E_{\nu}^k S_Q(E) dE = \sum_{\nu > 0} (\hbar\omega_{\nu})^k \left| \langle \nu | \hat{Q} | 0 \rangle \right|^2 \quad (2.9.5)$$

One can write the strength function in terms of the Fourier transform  $F(t)$  as

$$S_Q(E) = \frac{1}{2\pi} \int_{-\infty}^{+\infty} dt e^{-itE} F(t) \quad (2.9.6)$$

where the characteristic function  $F(t)$  [48] is given by

$$F(t) = \sum e^{-itE_\nu} \left| \langle \nu | \hat{Q} | 0 \rangle \right|^2 = m_0 + \frac{it}{1!} m_1 + \frac{(it)^2}{2!} m_2 + \dots \quad (2.9.7)$$

We can write, for  $k$  integer and positive,  $m_k$  as a ground state expectation value

$$m_0 = \langle 0 | Q^2 | 0 \rangle$$

Here we are interested in expressions for the odd moments  $m_1$  and  $m_3$ . For the arbitrary positive integer  $k$  and multipole operator  $\hat{Q}$  one can write the moments  $m_k$  as

$$m_k = (-)^t (i)^k \langle 0 | Q_s \cdot Q_t | 0 \rangle \quad (2.9.8)$$

with

$$Q_s = [iH, [iH, \dots, [iH, Q] \dots]] \quad (2.9.9)$$

where  $s$  is the number of times the Hamiltonian appears in (2.9.9) and  $s, t$  are arbitrary integers but such that their sum  $s + t = k$ . For the odd moments equation (2.9.8)

can also be written as [48]

$$m_k = \frac{1}{2} (-)^t (i)^k \langle 0 | [Q_s, Q_t] | 0 \rangle \quad (2.9.10)$$

which provides a very useful simplification of the structure of the operators whose expectation value one has to compute. The expectation values of moments clearly depend on the explicit form of the operator  $Q$ . The expectation values of odd moments  $m_1, m_3, m_5, \dots$  are written in terms of one body operators and are comparatively little model dependent. In contrast, the even moments  $m_0, m_2, m_4, \dots$  are written in terms of anticommutators and involve the expectation values of two body operators. We do not need the even moments. The high  $k$  moments are very sensitive to the form of potential and one must be careful to make an approximation. From expression (2.9.9) one can write

$$Q_1 = [iH, Q] = i[H, Q]$$

$$Q_2 = [iH, [iH, Q]] = -[H, [H, Q]] = [[H, Q], H]$$

Now using  $Q_1$  and  $Q_2$  in expression (2.9.13) we can write the moments  $m_1$  and  $m_3$  as

$$\begin{aligned}
 m_1 &= \frac{1}{2} (-)^0 (i)^1 \langle 0 | [Q_1, Q_0] | 0 \rangle & (2.9.11) \\
 &= \frac{1}{2} i \langle 0 | [i [H, Q], Q] | 0 \rangle \\
 &= -\frac{1}{2} \langle 0 | [[H, Q], Q] | 0 \rangle \\
 &= \frac{1}{2} \langle 0 | [Q, [H, Q]] | 0 \rangle
 \end{aligned}$$

and

$$\begin{aligned}
 m_3 &= \frac{1}{2} (-)^1 (i)^3 \langle 0 | [Q_2, Q_1] | 0 \rangle & (2.9.12) \\
 &= \frac{1}{2} i \langle 0 | [[[H, Q], H], i [H, Q]] | 0 \rangle \\
 &= -\frac{1}{2} \langle 0 | [[[H, Q], H], [H, Q]] | 0 \rangle \\
 &= \frac{1}{2} \langle 0 | [[H, Q], [[H, Q], H]] | 0 \rangle
 \end{aligned}$$

The moment  $m_3$  is finite and model independent . It depends only on the total electronic density. Expressions (2.9.11) and (2.9.12) are the starting points to evaluate the sum-rules.

What are the physical observables relevant to vibrational dynamics? Fundamental are the density and the excitation operators, whose expectation values give us the information about the position, momentum, energy etc of the particles. Up to here we have discussed and derived the general form of the different moments. Their values, however, clearly depend on the explicit form of the excitation operator  $\hat{Q}$ . In order

to analyze strength distributions and sum rules, one must therefore wisely design the precise form of  $\hat{Q}$ . In order to study the coupling of surface and volume plasmons for all multipolarities we choose here a set of trial operators

$$Q_L^p = r^p Y_{L,0}(\theta, \phi) \quad \text{with } p \geq L \quad (2.9.13)$$

with  $p$  being a positive real number. We therefore study the coupling of modes obtained with (2.9.13) using an increasing sequence of  $p$  value until convergence has been reached.

We now turn to the discussion of a scaling approach which is generalized by introducing several collective variables  $\alpha_\lambda$ , which are deduced from physical and symmetry deliberations, and construct the matching velocity fields. Any collective motions are expressed by letting  $\alpha_\lambda$  vary in time. To study the energy spectrum for the shape oscillations of the system one can start with by specifying the radius  $R(\theta)$  as a function of the angles. For axially symmetric deformations we need to consider only the  $\theta$ -dependence, so  $R(\theta)$  is characterized by the set of deformation parameters  $\alpha_\lambda$  in the multipole expansion [49]

$$R(\theta) = R_0 \left\{ 1 + \sum_{\lambda} \alpha_{\lambda}^* Y_{\lambda}(\theta) + O(\alpha^2) \right\} \quad (2.9.14)$$

where  $R_0$  is the radius of the system if it were spherical and the  $Y_{\lambda}$  are the spherical harmonics representing the successive surface modes produced by some disturbance.

In contrast to the early liquid drop model, the density of the system is not restricted to

be constant throughout. If the density of the system maintains the radial shape as it oscillates, then the expression for  $R(\theta)$  (2.9.14) applies to each equi-density surface. Such modes of oscillation are often referred to as irrotational flow. Other modes of oscillation are of course possible, but require a different parametrization. The eigenmodes are then found by diagonalizing the corresponding collective Hamiltonian:

$$H_c(\alpha) = \frac{1}{2} \sum_{\lambda} (B_{\lambda} |\dot{\alpha}_{\lambda}|^2 + C_{\lambda} |\alpha_{\lambda}|^2) \quad (2.9.15)$$

Such a harmonic oscillator Hamiltonian has the well-known classical solution

$$\omega_{\lambda} = \sqrt{\frac{C_{\lambda}}{B_{\lambda}}} \quad (2.9.16)$$

where the phenomenological parameters  $B_{\lambda}$  and  $C_{\lambda}$  are the mass and restoring-force coefficients respectively. In the jellium approximation the ionic background is smeared out into a constant positive background charge. This is a standard approach in the theory of bulk metals [50] and the adaptation to a finite cluster is straightforward. From the bulk a finite element of constant positive charge is carved out. The roughest approach is a homogeneously charged sphere with sharp surface. More versatile, more realistic and still easy to handle is a Wood-Saxon profile for the jellium density.

$$\rho(r) = \rho_0 \left[ 1 + \exp\left(\frac{r-R}{\alpha}\right) \right]^{-\gamma} \quad (2.9.17)$$

The possible deformations are parametrized in  $R(\theta)$  through the coefficient  $\alpha_{\lambda}$ . The

most significant of these is  $\alpha_2$  which produces axially symmetric deformation, where the positive values of  $\alpha_2$  leads to prolate (cigar-like shape as show in figure 6a) and negative values to oblate (pancake-like shape as shown in figure 6b).

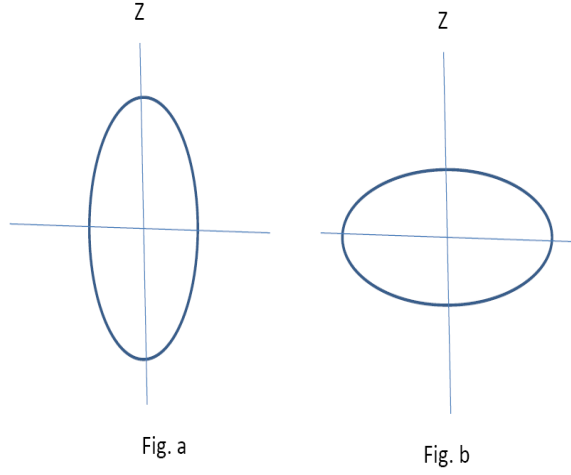


Figure 6: (a) The prolate charge distribution, which results in a positive value of electric quadrupole moment  $Q$ . (b) The oblate charge distribution, which results in a negative value of  $Q$ .

### 2.1.11 Evaluation of sum-rules

A widely used energy weighted sum-rule is given as

$$m_k(Q) = \sum_{\nu>0} (\hbar\omega_\nu)^k \left| \langle \nu | \hat{Q} | 0 \rangle \right|^2 \quad (2.10.1)$$

where  $k$  is an integer. In finite systems, we have to anticipate a coupling of surface and volume plasmons for all multipolarities. By using several values of  $p$  we incorporate a multidimensional extension of the sum rule approach. As discussed in reference [37],

$E_3$  is the one-phonon energy of a harmonic oscillator with spring constant  $C = m_3$  and mass  $B = m_1$ , which is the natural extension of equations (2.9.14) and (2.9.15) to introduce the following matrices:

$$B_{PP'} = \frac{1}{2} \langle 0 | [Q_L^P, [H, Q_L^{P'}]] | 0 \rangle \quad (2.10.2)$$

$$C_{PP'} = \frac{1}{2} \langle 0 | [[H, Q_L^P] [H, Q_L^{P'}], H] | 0 \rangle \quad (2.10.3)$$

Starting with equation (2.10.2), one can write;

$$B_{PP'} = \frac{m}{2\hbar^2} \int \vec{u}_L^P(\vec{r}) \cdot \vec{u}_L^{P'}(\vec{r}) \rho(\vec{r}) d^3r \quad (2.10.4)$$

with

$$\begin{aligned} \vec{u}_L^P(\vec{r}) &= -\frac{\hbar^2}{m} \nabla Q_L^P(\vec{r}) \\ \nabla &= \hat{r} \frac{\partial}{\partial r} + \hat{\theta} \frac{1}{r} \frac{\partial}{\partial \theta} + \hat{\phi} \frac{1}{r \sin \theta} \frac{\partial}{\partial \phi} \end{aligned}$$

so that expression (2.10.4) can be written as

$$\begin{aligned} B_{PP'} &= \frac{m}{2\hbar^2} \int \left[ -\frac{\hbar^2}{m} \nabla Q_L^P(\vec{r}) \right] \cdot \left[ -\frac{\hbar^2}{m} \nabla Q_L^{P'}(\vec{r}) \right] \rho(\vec{r}) d^3r \quad (2.10.5) \\ &= \frac{m}{2\hbar^2} \left( \frac{\hbar^2}{m} \right)^2 \int (\nabla Q_L^P(\vec{r})) \cdot (\nabla Q_L^{P'}(\vec{r})) \rho(\vec{r}) d^3r \\ &= \frac{\hbar^2}{2m} \int (\nabla Q_L^P(\vec{r})) \cdot (\nabla Q_L^{P'}(\vec{r})) \rho(\vec{r}) d^3r \end{aligned}$$

where,

$$\begin{aligned}
\nabla Q_L^P(\vec{r}) &= \nabla [r^P Y_{L,0}(\theta, \phi)] \\
&= \left( \hat{r} \frac{\partial}{\partial r} + \hat{\theta} \frac{1}{r} \frac{\partial}{\partial \theta} \right) (r^P Y_{L,0}(\theta)) \\
&= \hat{r} P r^{P-1} Y_{L,0}(\theta) + \hat{\theta} r^{P-1} \frac{\partial}{\partial \theta} Y_{L,0}(\theta)
\end{aligned}$$

Similarly

$$\nabla Q_L^{P'}(\vec{r}) = \hat{r} P' r^{P'-1} Y_{L,0}(\theta) + \hat{\theta} r^{P'-1} \frac{\partial}{\partial \theta} Y_{L,0}(\theta)$$

Therefore,

$$\begin{aligned}
(\nabla Q_L^P(\vec{r})) \cdot (\nabla Q_L^{P'}(\vec{r})) &= \left[ \hat{r} P r^{P-1} Y_{L,0}(\theta) + \hat{\theta} r^{P-1} \frac{\partial}{\partial \theta} Y_{L,0}(\theta) \right] \cdot \\
&\quad \left[ \hat{r} P' r^{P'-1} Y_{L,0}(\theta) + \hat{\theta} r^{P'-1} \frac{\partial}{\partial \theta} Y_{L,0}(\theta) \right] \\
&= P P' r^{P+P'-2} (Y_{L,0}(\theta))^2 + r^{P+P'-2} \left( \frac{\partial}{\partial \theta} Y_{L,0}(\theta) \right)^2 \\
&= r^{P+P'-2} \left[ P P' (Y_{L,0}(\theta))^2 + \left( \frac{\partial}{\partial \theta} Y_{L,0}(\theta) \right)^2 \right]
\end{aligned}$$

And

$$[Y_{L,0}(\theta)]^2 = \frac{2L+1}{4\pi} [P_L(\cos \theta)]^2$$

where  $P_L(\cos \theta)$  indicates the Legendre polynomial of order  $L$ .

Again

$$\begin{aligned}
\frac{\partial}{\partial \theta} Y_{L,0}(\theta) &= \sqrt{\frac{2L+1}{4\pi}} \frac{\partial}{\partial \theta} P_L(\cos \theta) \\
&= \sqrt{\frac{2L+1}{4\pi}} (-\sin \theta) \frac{\partial}{\partial (\cos \theta)} P_L(\cos \theta) \\
&= -\sqrt{\frac{2L+1}{4\pi}} \sin \theta \frac{L \cos \theta P_L(\cos \theta) - L P_{L-1}(\cos \theta)}{\sqrt{1 - \cos^2 \theta}}
\end{aligned}$$

Thus equation (2.10.5) can be written as

$$\begin{aligned}
B_{PP'} &= \frac{\hbar^2}{2m} \int r^{P+P'-2} \left[ PP' (Y_{L,0}(\theta))^2 + \left( \frac{\partial}{\partial \theta} Y_{L,0}(\theta) \right)^2 \right] \rho(\vec{r}) d^3r \\
&= \frac{\hbar^2}{2m} \int r^{P+P'-2} PP' [Y_{L,0}(\theta)]^2 \rho(\vec{r}) r^2 \sin \theta d\theta d\phi dr + \\
&\quad \frac{\hbar^2}{2m} \int r^{P+P'-2} \left[ \frac{\partial}{\partial \theta} Y_{L,0}(\theta) \right]^2 \rho(\vec{r}) r^2 \sin \theta d\theta d\phi dr \\
&= \frac{\hbar^2}{2m} PP' \int [Y_{L,0}(\theta)]^2 \sin \theta d\theta d\phi \int_0^\infty r^{P+P'} \rho(\vec{r}) dr + \\
&\quad \frac{\hbar^2}{2m} \int \left[ \frac{\partial}{\partial \theta} Y_{L,0}(\theta) \right]^2 \sin \theta d\theta d\phi \int_0^\infty r^{P+P'} \rho(\vec{r}) dr
\end{aligned}$$

But

$$\begin{aligned}
\int_{\theta=0}^{\pi} \int_{\phi=0}^{2\pi} Y_L^m Y_{L'}^{m'} d\Omega &= \frac{4\pi}{2L+1} \delta_{LL'} \delta_{mm'} \\
\therefore \int [Y_{L,0}(\theta)]^2 \sin \theta d\theta d\phi &= \int_{\theta=0}^{\pi} \int_{\phi=0}^{2\pi} Y_{L,0}(\theta) Y_{L',0}^*(\theta) d\Omega = \frac{4\pi}{2L+1}
\end{aligned}$$

To simplify these expression we have used the following formula as seen in [51]

$$\frac{\partial^\alpha}{\partial \theta} Y_{L,0}(\theta) = \sum_{L=1}^N [L(L+n-1)]^{\frac{\alpha}{2}} Y_{L,0}(\theta)$$

where  $\frac{\partial^\alpha}{\partial \theta}$  is the operator of fractional differentiation.

$$\begin{aligned}\frac{\partial}{\partial \theta} Y_{L,0}(\theta) &= [L(L+2-1)]^{\frac{1}{2}} Y_{L,0}(\theta) \\ &= [L(L+1)]^{\frac{1}{2}} Y_{L,0}(\theta)\end{aligned}$$

So

$$\left[ \frac{\partial}{\partial \theta} Y_{L,0}(\theta) \right]^2 = L(L+1) [Y_{L,0}(\theta)]^2$$

$$\int \left[ \frac{\partial}{\partial \theta} Y_{L,0}(\theta) \right]^2 \sin \theta d\theta d\phi = L(L+1) \frac{4\pi}{2L+1}$$

Hence

$$\begin{aligned}B_{PP'} &= \frac{\hbar^2}{2m} \left[ PP' \frac{4\pi}{2L+1} + L(L+1) \frac{4\pi}{2L+1} \right] \int_0^\infty r^{P+P'} \rho(\vec{r}) dr \\ \text{or } B_{PP'} &= \frac{\hbar^2}{2m} \frac{PP' + L(L+1)}{2L+1} (4\pi) \int_0^\infty r^{P+P'} \rho(r) dr\end{aligned}\quad (2.10.6)$$

Coupling of  $M$  multipole operators of the basis set (2.9.13) with  $L = 1, 2, \dots$  and  $P = 1, 2, \dots, M$ , ( $P \geq M$ ), we obtained the following mass parameter for the ingredients of the characteristic equation (3.2.12) discussed in section three

$$B_{PP'} = \left( \frac{\hbar^2}{2m} \right) \frac{PP' + L(L+1)}{2L+1} NR^{(P+P'-2)}\quad (2.10.7)$$

where

$$\int \rho(\vec{r}) d^3r = N$$

is the number of valence electrons present in the fullerene molecules. The details of the calculation is presented in appendix A.

The restoring force parameter defined in equation (2.10.4) can be rewritten as

$$\begin{aligned} m_3 [Q_L] &= C_{PP} = \frac{1}{2} \langle 0 | \left[ [H, Q_L^P] \left[ [H, Q_L^{P'}], H \right] \right] | 0 \rangle \\ &= \frac{d^2}{d\alpha d\alpha'} \left[ \langle 0 | e^{\alpha S_L^p} \hat{H} e^{-\alpha' S_L^{p'}} | 0 \rangle \right]_{\alpha=\alpha'=0} \\ &= \frac{d^2}{d\alpha d\alpha'} \left[ \langle \alpha | \hat{H} | \alpha' \rangle \right]_{\alpha=\alpha'=0} \end{aligned}$$

where

$$|\alpha\rangle = e^{-\alpha S_L^p} |0\rangle$$

is called the scaled ground state. Now one can write

$$C_{pp'} = C_{pp'}^{kin} + C_{pp'}^{xc} + C_{pp'}^{Coul} + C_{pp'}^{V_I}$$

The contributions from the coulomb interaction  $C_{pp'}^{Coul}$  and from the external jellium potential  $C_{pp'}^{V_I}$  are calculated in appendix. Without the kinetic energy part and the exchange correlation contribution, the restoring force parameter is evaluated as:

$$C_{PP'} = \left( \frac{\hbar^2}{m} \right)^2 \frac{N^2 e^2}{(2L+1)} \left( R^{(P+P'-5)} \right) \left[ \frac{R}{2\Delta} P P' + \frac{L(L+1)}{2(2L+1)} (2L^2 + 2L - P - P' - 2PP') \right]$$

The kinetic energy and the exchange correlation contributions have been evaluated in the local density approximation (LDA).

## 3 Chapter

### 3.1 Coupling of surface and volume plasmons in fullerene molecules

#### 3.1.1 Introduction

In 1947, Baldwin and Klaiber established the existence of strong resonances in nuclear photo-absorption cross sections. In fact, such resonance behavior had previously been predicted by A. B. Migdal [52]. The first indications of a giant dipole resonance (GDR) were obtained experimentally by Bethe and Gentner (1937). Very soon it was found that these giant resonances are a general feature of most nuclei. The form and width of the resonance change only smoothly with the particle number. The resonances turned out to be of electric dipole character. Goldhaber and Teller [20] and Steinwedel and Jensen [24] explained this effect as a collective vibration of protons against neutrons. The restoring force against the separation of protons from neutrons is the symmetry energy which also enters into the semi-empirical mass formula. It is the volume symmetry energy in the case of the Steinwedel-Jensen model and the surface symmetry energy in the case of Goldhaber-Teller model. In a simplified model (Goldhaber-Teller), one considers the oscillations of the non-deformed neutron sphere against the non-deformed proton sphere. A dependence of the centroid energy of the form  $E_c \propto A^{-\frac{1}{6}}$  was obtained [24]. Here A indicates the number of nucleons. The same authors also proposed the more sophisticated two-fluid model which was finally

worked out by Steinwedel and Jensen. In this model, one obtains an A-dependence of the centroid energy of  $E_c \propto A^{-\frac{1}{3}}$ . Neither of the two models agrees completely with the experimental findings. Detailed analysis of experimental data showed that a suitable combination of both models was necessary to interpret these data so that the GDR could be best understood in terms of coupled translational and compressional dipole modes. These early and somewhat crude classical models were later refined by a quantized fluid dynamics approach [53]. Several researchers [54][3][55] applied these semiclassical models successfully to clusters where a similar coupling between translational and compressional dipole modes has been observed [37],[56],[57].

The computation of the collectively excited states of the fullerene molecule  $C_{60}$  follows this trend. It is now well understood that the optical resonance of  $C_{60}$  is a collective excitation similar to the plasmon resonance in the bulk or the giant resonances in nuclear matter. In this chapter it is shown that the local current approximation (LCA) which encompasses both the fluid-dynamical and sum rule approaches can be derived from a variational principle. Starting with the equation of motion, the LCA has been applied to study the collective electronic excitations in  $C_{60}$  molecules. Recent studies [14] by Scully et al of the optic response of  $C_{60}$  molecules have revealed both a surface and a volume plasmon. The latter shows up as a broad high-energy shoulder in the photo-ionization cross section which again can be semiclassically understood as a compressional component of the collective dipole excitation.

### 3.1.2 Electrostatic potential of a uniformly charged spherical shell

Let us consider a spherical shell of fullerene molecules as shown in figure 7.

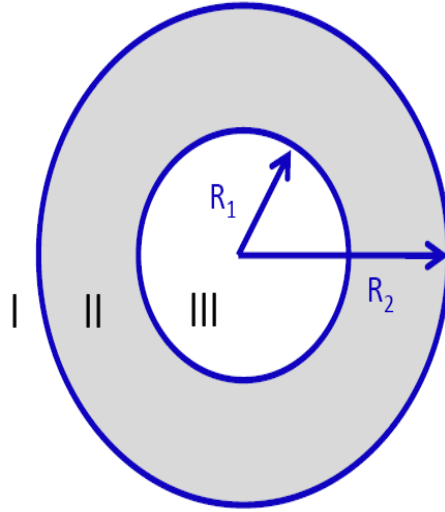


Figure 7: Schematic representation of fullerene molecules shell.

Suppose  $R_1$  is the inner radius and  $R_2$  is the outer radius of the shell. If  $E_1$ ,  $E_2$  and  $E_3$  are the electric intensity in three different regions of the shell as shown in the figure, 7, then

$$\vec{E}_{III} = 0 \text{ for } r \leq R_1$$

$$\vec{E}_I = \frac{Q}{4\pi\epsilon_0 r^2} = \frac{\rho_0}{3\epsilon_0} [R_2^3 - R_1^3] \frac{\hat{r}}{r^2} \text{ for } r > R_2$$

$$\vec{E}_{II} = \frac{4\pi}{3} \frac{1}{4\pi\epsilon_0} [r^3 - R_1^3] \frac{\hat{r}}{r^2} = \frac{\rho_0}{3\epsilon_0} \left[ 1 - \frac{R_1^3}{r^3} \right] \vec{r} \text{ for } R_1 \leq r \leq R_2$$

By evaluating the corresponding electrostatic potentials of shell as follows:

$$\phi_I = - \int_{\infty}^r \frac{\rho_0}{3\epsilon_0} [R_2^3 - R_1^3] \frac{1}{r^3} \vec{r} \cdot d\vec{r} = \frac{\rho_0}{3\epsilon_0} [R_2^3 - R_1^3] \frac{1}{r}$$

$$\begin{aligned} \phi_{II} &= \phi_1(R_2) - \int_{\infty}^r \frac{\rho_0}{3\epsilon_0} \left[ 1 - \frac{R_1^3}{r^3} \right] \vec{r} \cdot d\vec{r} \\ &= \frac{\rho_0}{3\epsilon_0} \left[ R_2^2 - \frac{R_1^3}{R_2} \right] - \left[ \frac{\rho_0}{3\epsilon_0} \frac{r^2}{2} + \frac{\rho_0}{3\epsilon_0} \frac{R_1^3}{r} \right]_{R_2} \\ &= \frac{\rho_0}{3\epsilon_0} \left[ \frac{3}{2} R_2^2 - \frac{r^2}{2} - \frac{R_1^3}{r} \right] \end{aligned}$$

$$\phi_{III} = \phi_2(R_1) = \frac{\rho_0}{3\epsilon_0} \frac{3}{2} [R_2^2 - R_1^2]$$

### 3.1.3 Simple Models for Plasmon Oscillations:

A neutral plasma is a medium with equal number of positive and negative charges of which at least one charge is mobile. In a solid the negative charges of the conduction electrons are balanced by an equal number of positive charge of the ion cores. A plasma oscillation is a collective periodic excitation of an electron gas. The quantized plasma oscillation is called a plasmon, where the electron gas moves as a whole with respect to the positive ionic background.

Experimentally the plasmons were first recognized in the collision of low-energy electrons and thin conducting metallic film. In this experiment the scattered electrons

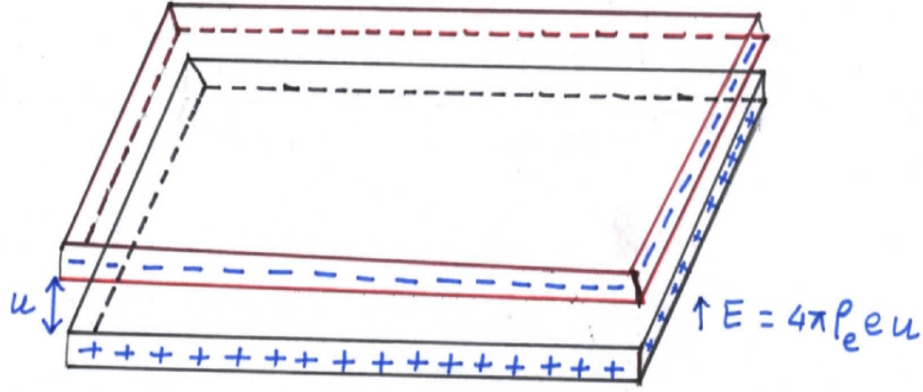


Figure 8: Plasmon in a thin metallic films

experience energy losses equal to multiples of the plasmon energy [58]. In this case the excitation may be simply understood by considering a longitudinal plasma oscillation as show in figure 8 as a uniform displacement of an electron gas in a thin metallic slab. The electron gas is moved as a whole with respect to the positive ion background. A displacement of the electron gas of amplitude  $u$  perpendicularly to the surface creates an electric field  $E = 4\pi\rho_e eu$ , where  $e$  and  $\rho_e$  are electron charge and the density of electron, that acts as a restoring force, proportional to the displacement  $u$ , on the gas[59]. One can derive the equation of motion of unit volume of the electron gas using Newton's second law of motion as;

$$\rho_e m_e \frac{d^2 u}{dt^2} = -\rho_e e E = -4\pi\rho_e^2 e^2 u$$

$$\frac{d^2 u}{dt^2} + \omega_p^2 u = 0; \quad \omega_p = \sqrt{\frac{4\pi\rho_e e^2}{m_e}}$$

where  $m_e$  is the electron mass and  $\omega_p$  is called the plasma frequency. This simple model for plasmon oscillations in a thin metallic slab can be applied to the fullerene shell where the electron shell oscillates against the positive ionic background as shown in figure 9.

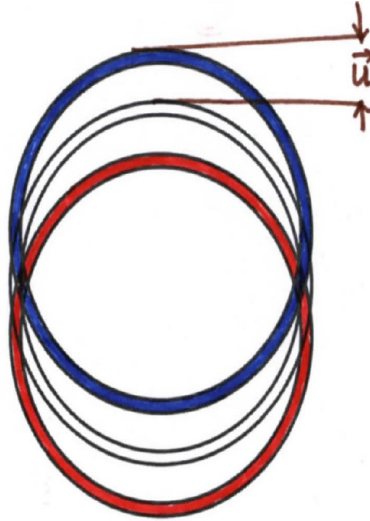


Figure 9: Movement of plasmon in fullerene molecules

Such a periodic displacement of the electron shell may be resonantly excited by an external field, keeping the system as a whole electrically neutral, consequently a time varying electric dipole is observed.

#### 3.1.4 Spherical Jellium Model

Puska and Nieminen [60] introduced the spherical shell model for the  $C_{60}$  molecule. They introduced a shell of positive rigid background charge, jellium, which symmetrically placed with respect to the radius  $R$  of the  $C_{60}$  molecule. In the spherical jellium model, the ionic background density  $\rho_I(r)$  is that of a uniformly charged sphere with

radius  $R_I$  :

$$\rho_I(r) = \rho_0 \Theta(r - R_I)$$

The size of the jellium is determined by the number of ions  $N$  present in the jellium. In our model we matched the electronic density to an ionic density expressed by step functions

$$\rho_I(r) = \rho_0 [\Theta(R_2 - r) - \Theta(r - R_1)]$$

where  $R_1$  and  $R_2$  are the inner and outer radii of the shell. To improve the jellium model, the use of pseudopotentials has been introduced but is not the part of the present work. The jellium model can be applied to large clusters with thousands of atoms where more structural models may not be possible.

### 3.1.5 Local Current Approximation (LCA):

The purpose of this work is the calculation of excited collective states of fullerenes following the methods outlined above. From the equation of motion (2.8.1) and (2.8.2) the following variational principle can be derived [36]: Solving the equation of motion (2.8.1) with condition (2.8.2) for the lowest excited state is equivalent to solving the variational equation

$$\frac{\delta E_\nu [\hat{Q}]}{\delta \hat{Q}} = 0 \tag{3.1.1}$$

where  $E_\nu$  for  $\nu = 3$  is defined by

$$E_3 [\hat{Q}] = \sqrt{\frac{m_3 [\hat{Q}]}{m_1 [\hat{Q}]}}$$

and the moments  $m_1$  and  $m_3$  are defined as the multiple commutators

$$m_1(\hat{Q}) = \frac{1}{2} \langle 0 | [\hat{Q}, [\hat{H}, \hat{Q}]] | 0 \rangle \quad (3.1.2)$$

$$m_3(\hat{Q}) = \frac{1}{2} \langle 0 | [[\hat{H}, \hat{Q}], [\hat{H}, [\hat{Q}, \hat{H}]]] | 0 \rangle \quad (3.1.3)$$

The exact operator  $\hat{Q}$  is not known. It has to be Hermitean and is generally nonlocal. It can be viewed as a generalized coordinate. The values of the moments, however, depend on the explicit form of  $\hat{Q}$ . So we need a convenient set of approximate operator function  $Q_L(\vec{r})$  which will be defined later.

The excitation spectrum can be produced by successive orthogonalizations of  $\hat{Q}$ . In the fluid dynamical approach, one approximates the collective excitation energies  $\hbar\omega_\nu$  by the energy  $E_3[\hat{Q}_\nu]$  with  $\nu$  indicating a particular excitation energy. In the LCA one starts either from the uncorrelated Hartree-Fock or Kohn-Sham ground state  $|0\rangle$  and takes the operator  $\hat{Q}$  as a local function  $Q(\vec{r})$ , to calculate the following moments:

$$m_1(\hat{Q}) = \frac{1}{2} \langle 0 | [\hat{Q}, [\hat{H}, \hat{Q}]] | 0 \rangle = \frac{m}{2\hbar^2} \int u(\vec{r}) \cdot u(\vec{r}) \rho(\vec{r}) d^3r \quad (3.1.4)$$

with

$$u(\vec{r}) = -\frac{\hbar^2}{m} \nabla Q(\vec{r})$$

where  $u(\vec{r})$  is a local displacement field to be determined by the Rayleigh-Ritz variational principle. It is proportional to the collective current

$$\vec{j}_\alpha(\vec{r}, t) = \rho_\alpha(\vec{r}, t) \vec{v}_\alpha(\vec{r}, t)$$

with

$$\vec{v}_\alpha(\vec{r}, t) = \alpha_p(t) \vec{u}(\vec{r})$$

which obey the continuity equation:

$$\frac{\partial}{\partial t} \rho_\alpha(\vec{r}, t) + \nabla \cdot \vec{j}_\alpha(\vec{r}, t) = 0$$

Here  $\rho_\alpha(\vec{r}, t)$  are "scaled" time dependent densities. Note that if  $\nabla^2 Q(\vec{r}) = 0$  and thus  $\vec{\nabla} \cdot \vec{u}(\vec{r})$  vanishes, then one has incompressible collective flow; otherwise the collective motion incorporates also local compressions of the fermi fluid.

As an illustration, we consider the displacement field for a multipole surface vibration. This is obtained by having a field of the form  $\vec{\nabla} r^L P_L(\cos \theta)$ , with  $P_L$  a Legendre polynomial of angular momentum  $L$ . The incompressibility then follows from the relation

$$\vec{\nabla} \cdot \vec{u}(\vec{r}) = \nabla^2 r^L P_L(\cos \theta) = 0$$

Any flow generated by such a potential field is also irrotational. The moment  $m_3(Q)$  defined in (3.1.3) is a more complicated functional of  $\vec{u}(\vec{r})$ , of the spatial density  $\rho(\vec{r}) = \sum_{i=1}^N |\phi_i(\vec{r})|^2$  and of the kinetic energy density  $\tau(\vec{r}) = \sum_{i=1}^N |\nabla\phi_i(\vec{r})|^2$  given here in terms of the ground state HF or KS wave functions  $\phi_i(\vec{r})$ .

For an intuitive understanding how  $\frac{\delta E_3[Q]}{\delta Q(\vec{r})} = 0$  can be solved approximately, it helps to recall the scaling model of nuclear physics [49]. In this model, the energy  $E_3[\hat{Q}] = \sqrt{\frac{m_3[\hat{Q}]}{m_1[\hat{Q}]}}$  is interpreted corresponding to a scaling transformation

$$|\phi_n\rangle = e^{-i\eta S} |\phi_0\rangle \quad (3.1.5)$$

with respect to the collective Hamiltonian

$$H_{\text{col}} = \frac{1}{2} \sum (B_{pp'} \dot{\eta}_p \dot{\eta}_{p'} + C_{pp'} \eta_p \eta_{p'}) \quad (3.1.6)$$

where  $\eta$  is a harmonically oscillating arbitrary scalar parameter and the scaling operator is defined by

$$\hat{S} = [\hat{H}, \hat{Q}_{ext}].$$

Then

$$m_3 = \frac{1}{2} \frac{\partial^2}{\partial \eta^2} \left[ \langle \phi_n | \hat{H} | \phi_n \rangle \right]_{\eta=0}$$

The energy weighted moment  $m_3$  measures the change of the energy of the system

when the ground state wavefunction is deformed according to expression (3.1.5). It is a finite quantity, given by the expectation value of a one-body operator and, thus, quite model independent. For clusters, it depends only on the total electronic density at the origin. For instance, if  $\hat{Q}_{ext}$  stands for the dipole operator  $\hat{Q} = z$ , the scaling transformation is just a translation along the z-axis. The variation  $\frac{\delta E_3[Q]}{\delta Q(\vec{r})} = 0$  leads to fluid dynamical eigenvalue equation:

$$\frac{\delta m_3[\vec{u}]}{\delta u_j(\vec{r})} = (\hbar\omega_\nu)^2 \frac{m}{\hbar^2} \rho(\vec{r}) \vec{u}_j(\vec{r}) \quad (3.1.7)$$

yielding the spectrum  $\hbar\omega_\nu$  and eigenmodes  $\vec{u}_\nu$ . A practical way to solve (3.1.7) approximately consists in representing the operator  $Q(\vec{r})$  in terms of a finite set of known basis functions  $\{Q_\lambda(\vec{r})\}$ :

$$Q(\vec{r}) = \sum_{p=1}^N c_p Q_L^p(\vec{r}) \quad \text{with} \quad Q_L^p = r^p Y_{L0}(\theta), \quad p = L, L+1, \dots, N \quad (3.1.8)$$

The first two multipole operators exciting surface vibrations are the dipole operator  $Q_d = r \cos \theta = z$  describing a purely translational mode and the quadrupole operator  $Q_2 = r^2 Y_{20}$  with a more structured oscillation pattern. The monopole operator  $Q_0(r) = r^2 Y_{00}$  effects a breathing mode but not a surface phonon. Such density changing modes can be obtained also for higher multipoles by setting the power  $p$  of the radial variable  $r^p$  to values higher than  $L$ . ([61] appendix).

The variational principle yields then a set of  $M$  secular equations with

$$\det |C_{pp'} - (\hbar\omega_\nu)^2 B_{pp'}| = 0, \quad (p, p', \nu = 1, 2, \dots, M) \quad (3.1.9)$$

as the characteristic equation. Here

$$B_{pp'} = \langle 0 | [Q_p, [\hat{H}, Q_{p'}]] | 0 \rangle \quad (3.1.10)$$

$$C_{pp'} = \frac{1}{2} \langle 0 | [[\hat{H}, Q_p], [\hat{H}, [Q_{p'}, \hat{H}]]] | 0 \rangle \quad (3.1.11)$$

By solving equation (3.1.9), one can find the excitation energies  $\hbar\omega_\nu$  of the system and can evaluate its response to an external excitation operator  $Q_{ext}$ . Details can be found in the appendix of reference [61].

The dipole mode describes the collective translational motion of the electrons relative to the ion core. The displacement field vector can be as simple as a uniform displacement field, rendering dipole modes which are relatively simple to construct and rather collective. The collectivity of the response causes a concentration of a large fraction of the oscillator strength in a small frequency interval. This is the origin of the name "giant dipole resonance" in nuclear physics, a term that is now applied to a corresponding bump that appears in the optical absorption spectrum of atoms, molecules and clusters [12], [62].

The quadrupole mode  $L = 2$  and higher modes are not excited by a single photon but in collision processes or multiphoton absorption.

It is thus possible to estimate the position and the width of a resonance mode, whose collective strength is concentrated in one peak, by calculating the sum rules (3.1.10) and (3.1.11). Having solved (3.1.9), we know the eigenmodes of the system and can compute its response to an external excitation operator  $Q_{ext}$ . To this purpose we define a strength function

$$S_{Q_{ext}}(E) = \sum_{\nu>1} \left| \langle \nu | \hat{Q} | 0 \rangle \right|^2 \delta(E - \hbar\omega_\nu) \quad (3.1.12)$$

whose energy weighted moments  $m_k(Q_{ext})$  become

$$m_k(Q_{ext}) = \int_0^\infty E^k S_{Q_{ext}}(E) dE = \sum_{\nu>1} (\hbar\omega_\nu)^k |\langle \nu | Q_{ext} | 0 \rangle|^2 \quad (3.1.13)$$

The photo-absorption cross section  $\sigma(\omega)$  in the long wavelength limit becomes

$$\sigma(\omega) = (4\pi\omega/3c) S_{dip}(E = \hbar\omega) \quad (3.1.14)$$

where  $Q_{ext} = Q_{dip} = ez$  is the dipole operator and  $\omega$  is the frequency of the external electric field. For application in metal clusters [37], the following basis set of local operators has successfully been used:

$$Q_L(\vec{r}) = er^p Y_{L0}(\theta) \quad (3.1.15)$$

where  $p = 1, 2, \dots, M$ . We consider here only dipole modes ( $L = 1$ ); for  $p = 1$  we then have the electric dipole operator  $Q_1 = Q_{dip} = ez$ , while for  $p > 1$  we obtain

compressional component of dipole modes with  $\nabla^2 Q_p \neq 0$ . Hence, a finite set with  $M \geq 2$  of these operators will allow for the description of coupled translational and vibrational dipole modes. When  $M > 1$  modes are coupled, one of which has  $p = 1$  (pure dipole mode) and all others have  $M - 1$  different but arbitrary real values  $p > 1$ , the spectrum always consists of one surface plasmon with frequency  $\omega = \omega_{Mie}$  and  $M - 1$  degenerate volume plasmons with the frequency  $\omega = \omega_{vol}$  [61]. Figure 10 below illustrates (a) the pure translational vibration of the electrons against the ions described by the single dipole operator  $Q_{dip} = ez$ . It leads to the so-called Mie Plasmon or the surface plasmon with energy

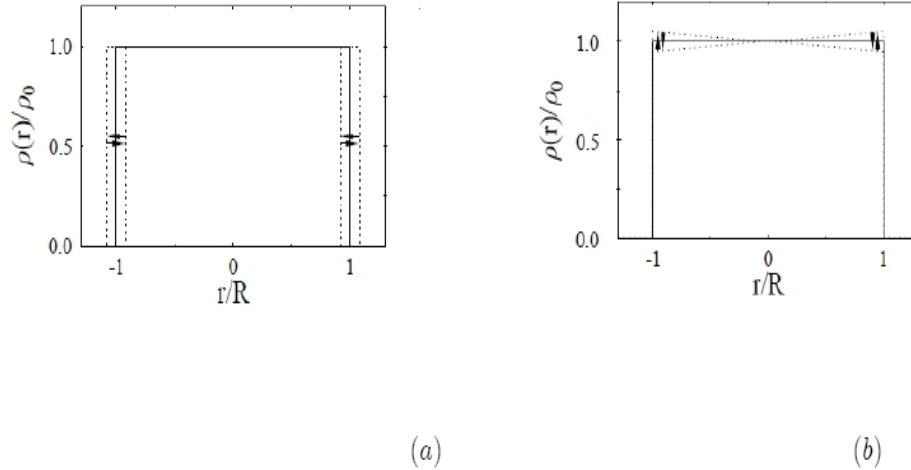


Figure 10: Schematic picture of collective oscillations of electrons (dotted lines) against ions (solid lines) in the spherical jellium model for a metal cluster. (a) pure translational, yielding the Mie surface plasmon (Goldhaber-Teller mode in nuclear physics). (b) compressional dipole mode, leading to a volume plasmon (Steinwedel-Jensen-Migdal mode in nuclei)

$$E_3(Q_d) = \hbar\omega_{Mie} = \sqrt{\frac{\hbar^2 e^2 N}{mR^3}} \quad (3.1.16)$$

where  $N$  is the number of particles. This what corresponds to the Goldhaber-Teller model for the nuclear isovector giant dipole resonance (GDR). (b) a compressional mode brought about by a suitable combination of operators (3.1.15) with  $p > 1$  which corresponds to the Steinwedel-Jensen mode for the nuclear GDR.

The frequency  $\omega_{vol}$  is the bulk plasma frequency  $\omega_{pl}$  of the corresponding metal

$$\omega_{vol} = \omega_{pl} = \sqrt{\frac{3e^2}{mr_s^3}} \quad (3.1.17)$$

where  $r_s$  is the Wigner-Seitz radius. This volume plasmon can also be brought about as a pure compressional mode by monopole operator  $Q_0 = er^2$ , which is also used to describe the nuclear breathing mode :

$$E_3(Q_0) = \hbar\omega_{vol} = \sqrt{\frac{3\hbar^2 e^2 N}{mR^3}} = \sqrt{3}\hbar\omega_{Mie} \quad (3.1.18)$$

This mode can not be excited by the external dipole operator since it corresponds to  $L = 0$ , and therefore does not couple simply to the electric dipole field. The surface plasmon with frequency  $\omega_{Mie}$  then carries all of the dipole strength.

### 3.2 Coupling of surface and volume dipole oscillations in fullerene molecules

The structure of  $C_{60}$  molecules is a truncated icosahedron, which resembles a soccer ball of the type made of twenty hexagons and twelve pentagons, with a carbon atom at the vertices of each polygon and a bond along each polygon edge as shown in figure 11.

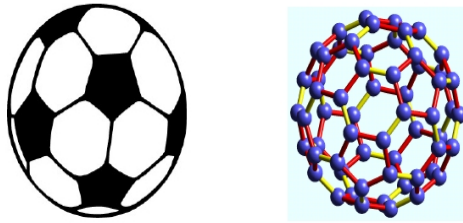


Figure 11: Comparison of the icosahedron structure of the fullerene molecules to that of a soccer ball.

The sixty carbon atoms, provided each four valence electrons, so that a total of  $N = 240$  electrons can oscillate collectively against the ionic background. Indeed, a giant resonance peak has been predicted by Bertsch and collaborators [12] in 1991 using linear-response theory. They found that the 240 valence electrons in the  $C_{60}$  molecules are delocalized and a giant collective plasmon resonance could be excited by an external electromagnetic field of  $\hbar\omega \sim 20 \text{ eV}$ . Very soon after their prediction was published Hertel and collaborators [13] experimentally observed a giant resonance in free  $C_{60}$  molecules. A strong, broad resonance centered around  $20 - 22 \text{ eV}$  was excited using monochromatic synchrotron radiation.

The first independent absolute cross-section measurements for photoionization of the fullerene molecules were reported by S. W. J Scully et al [14] in 2005. Their experiments on the optic response of the fullerene  $C_{60}$  molecules found the resonance peak at approximately the predicted position but also a broad shoulder around 30–45 eV which is interpreted as a volume plasmon. A two-Lorentzian fit to the single photoionization cross section located the surface plasmon at more accurately  $22 \pm 0.1eV$  and the volume plasmon at  $38 \pm 2eV$ .

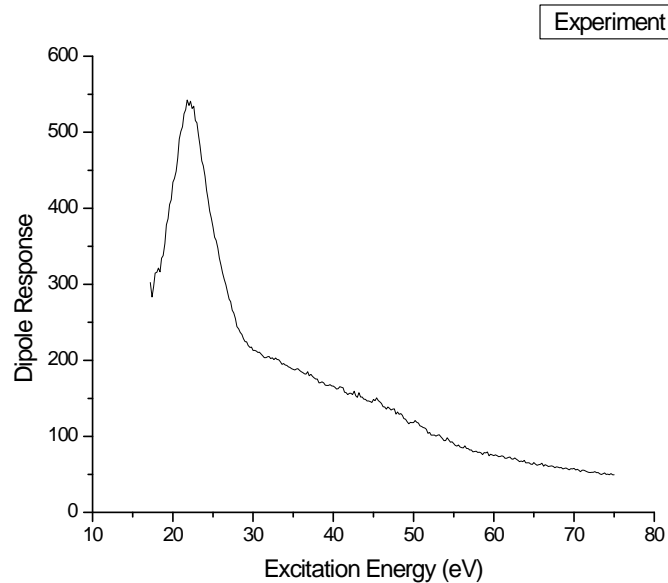


Figure 12: Optic response of  $C_{60}$  molecules; experimental photoionization cross section result

Two distinct modes: surface plasmon and volume plasmon, of collective oscillations of the 239 valence electrons of the  $C_{60}^+$  molecule due to photoexcitation [14] are shown in the figure 13.

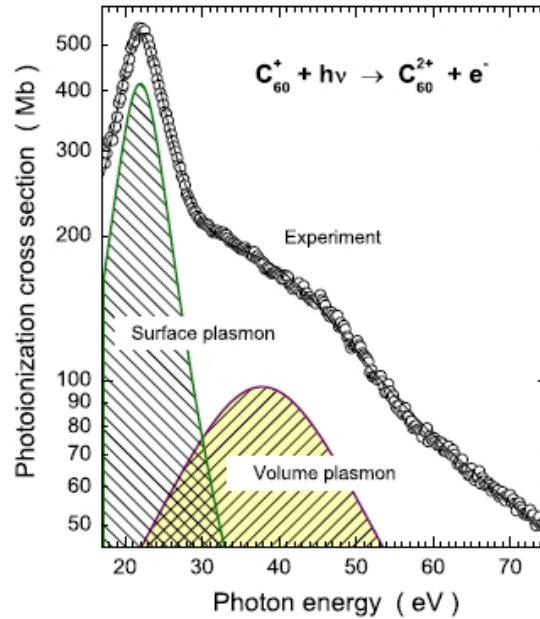


Figure 13: Surface and volume plasmon in  $C_{60}^+$  molecule

Figure 13 shows a fit of two Lorentzian curves to the measured cross section for single photoionization of  $C_{60}^+$ , clearly indicating two broad resonance features.

A time dependent local density approximation (TDLDA) calculation [63] reported by Rudel et al (see figure 14) used a readjusted version of the Jellium model [60]. It yielded an extra peak around 42 eV besides the main peak at 22 eV, without however shedding more light on the accurate nature of the corresponding collective motion. The interpretation of the peak at the higher energy as a compressional component of the collective motion appears to be accepted now [65] in spite of initial challenges [64].

In this work we have applied the framework of the local current approximation to the calculation of collective excitation by using the same electron density and ionic

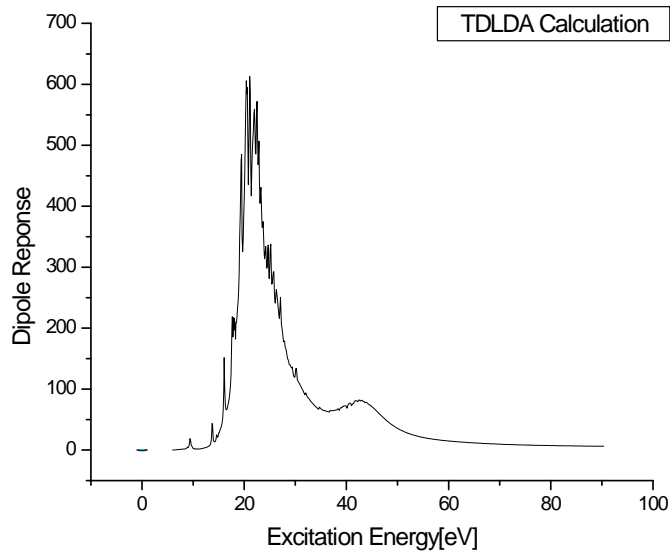


Figure 14: Optic response of  $C_{60}$  molecules; TDLDA calculation

background as in the calculation of Rudel to demonstrate the photoionization cross section and geometrical properties of valence electrons in many electron systems. We determine dipole excitation energies of  $C_{60}$  using exactly the same electron density as was used in the Berlin-Dresden collaboration of reference [63]. It is shown in figure 15.

This density is matched to an ionic density expressed by step functions

$$\rho_I(r) = \rho_0 [\Theta(R_2 - r) - \Theta(r - R_1)] \quad (3.2.1)$$

where  $R_1 = R - \frac{\Delta}{2}$ ,  $R_2 = R + \frac{\Delta}{2}$  are the inner and outer radii of the shell with  $\Delta$  as thickness of the shell presented in table 1.

The uniform ion density  $\rho_0$  is chosen such that the integrated ion charge is equal

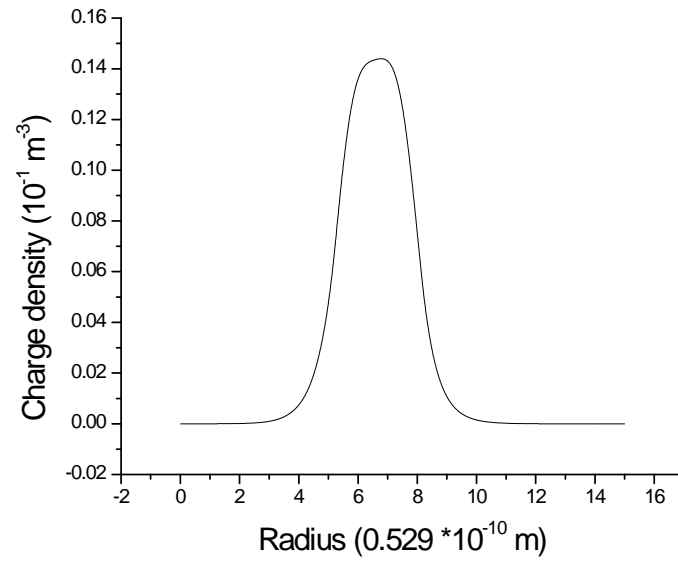


Figure 15: Density of electrons in fullerene  $C_{60}$  molecule.

$R$	0.354 nm
$R_1$	0.2775 nm
$R_2$	0.4305 nm
$\Delta$	0.153 nm

Table 1: Physical parameters for the fullerene molecule.

but of opposite sign to that of the valence electrons. We hold the ionic charge fixed and unaffected by the oscillations of the valence electrons (jellium model).

pure surface Plasmon ( $eV$ )	coupled surface plasmon ( $eV$ )	coupled volume plasmon ( $eV$ )
22.1 <sup>a</sup>	21.4 <sup>a</sup>	37 <sup>a</sup>
—	20 <sup>b</sup>	—
—	22 <sup>c</sup>	42 <sup>c</sup>
—	20 <sup>d</sup>	—
—	22 <sup>e</sup>	40 <sup>e</sup>
—	19 <sup>f</sup>	—

Table 2: The optic dipole response of fullerene molecules according to various theoretical and experimental studies.

*a*: LCA theoretical data (present work), *b*: Theoretical data [66]

*c*: TDLDA calculation [63], *d*: Experimental data [13], (data exhibits a flat structure from 15 to 25  $eV$ ), *e*: Experimental data [14], *f*: Experimental data [67]

Table 2 shows the theoretical and experimental optic dipole response of  $C_{60}$  molecules. In column two we have presented the theoretical and experimental coupled surface plasmon. Comparing with theoretical and experimental findings in column two, it is not difficult to conclude that the the giant dipole surface plasmon resonance of 240 delocalized valence electrons in the  $C_{60}$  molecules can be excited by an external electromagnetic field of  $\hbar\omega = 20 - 22 eV$ . However, the experimental result presented by Ju et al [67] is lower than 20  $eV$ . A first experimental result of such a dipole resonance [13] reported a strong broad resonance centered near 20  $eV$  (see figure 16). From the careful comparison between the experimental data reported by different experimentalists, it is found that the reported experimental results differ by  $\pm 2 eV$  in the case of the dipole translational mode. The experimental uncertainty is higher for the compressional dipole mode.

It is noteworthy to mention that recent theoretical work on the optic response of

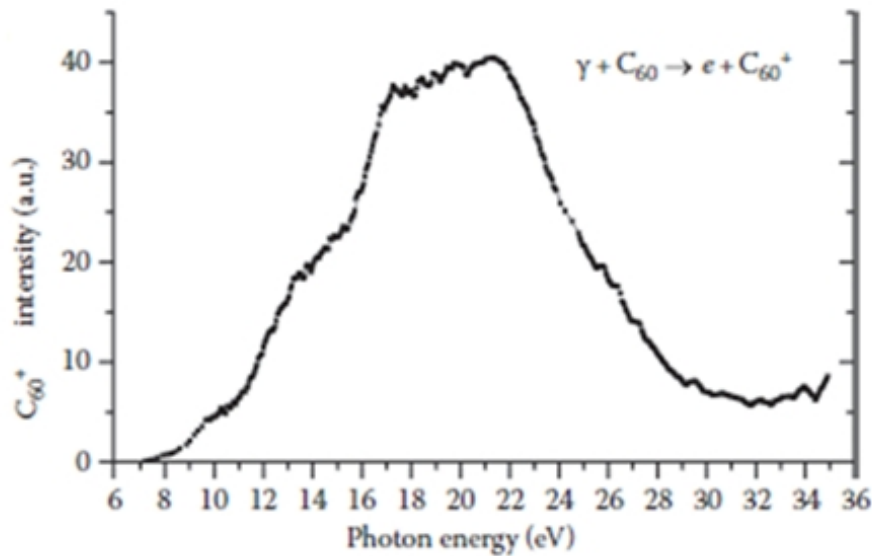


Figure 16: Photoionization experiments have been performed with  $C_{60}^+$  ions [13] and lead to excitation of the giant plasmon resonance.

$C_{60}$  molecules studied at higher energies found a broad shoulder around 30 – 45 eV which is interpreted as a volume plasmon. As an example of exploration of higher energy regime the theoretical LCA calculation of the volume plasmon along with surface plasmon of  $C_{60}$  molecules for the dipole mode is reported in figure 17 below. This feature is not seen as clearly in experimental data because of the broadness of the underlying structure. But its existence can be deduced indirectly by the observed shift of the resonance peak to lower energy which is a consequence of the coupling of volume and surface plasmons as shown in a number of theoretical studies.

Figure 18 represents the comparison of experimental and theoretical results. The circles represent the experimental data reported by Scully et al [14]. They observed

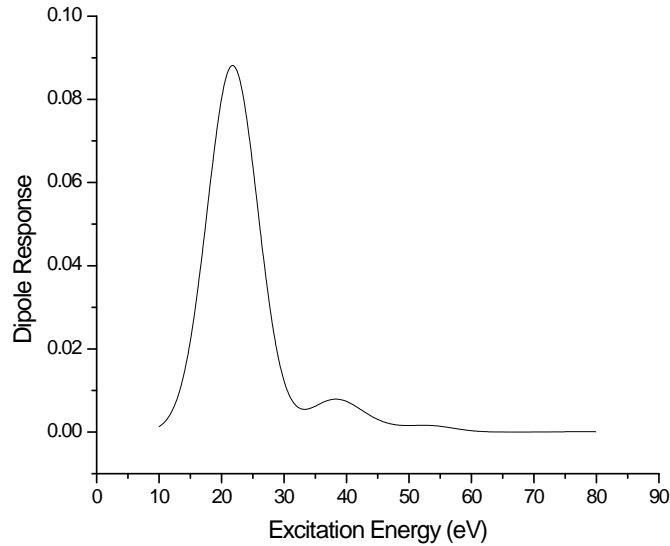


Figure 17: Optic response of  $C_{60}$  molecules : LCA calculation

the giant surface plasmon resonance near  $22\text{ eV}$  in their absolute photoionization measurement. They also observed a broad feature near  $40\text{ eV}$ , which is suggestive of a higher order plasma oscillation. The solid line represents the time dependent local density approximation (TDLDA) results. TDLDA calculation using jellium model yielded besides the surface peak at  $22\text{ eV}$ , an extra peak around  $42\text{ eV}$ , without, however, revealing the precise nature of the corresponding collective motion. Dashed line represents the LCA calculation. This approach uses the same jellium model as in TDLDA and the results support the experimental finding, i. e. giant surface plasmon at  $21.4\text{ eV}$  and the volume plasmon at  $37\text{ eV}$ .

To obtain the dipole mode with an energy we call  $E_3(Q_1)$  for reasons that will be explained below, one uses the dipole operator  $Q_1(\vec{r}) = rY_{10} = r \cos \theta = z$  which

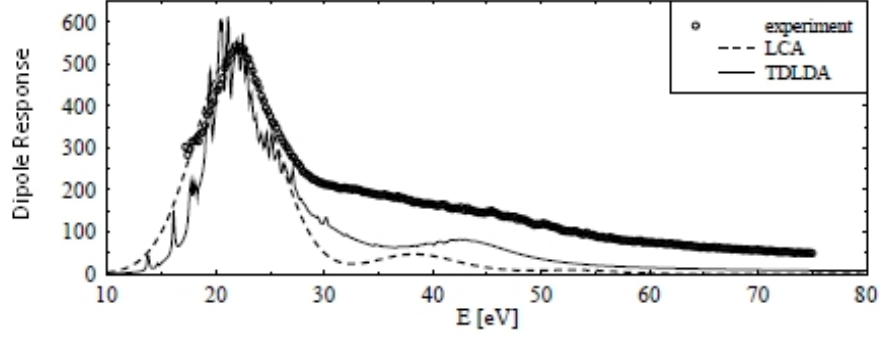


Figure 18: Comparison of optic response of  $C_{60}$  molecule. Circles: Experimental photoionization cross section [Scully et al]. Solid lines: TDLDA calculations [Rudel et al]. Dashed lines: present LCA calculation.

yields the surface plasmon at

$$E_3(Q_1) = \sqrt{\frac{\hbar^2 N e^2}{3mR^2\Delta}} = 21.4eV \quad (3.2.2)$$

where  $E_3$  is defined by

$$E_3[\hat{Q}] = \sqrt{\frac{m_3[\hat{Q}]}{m_1[\hat{Q}]}}$$

with multiple commutators  $m_1$  and  $m_2$ . The element of the mass parameter  $B_{PP'}$  and of the restoring force parameter  $C_{PP'}$  for the dipole case are given as

$$B_{PP'} = \left(\frac{\hbar^2}{m}\right) \frac{(PP'+6)}{6} NR^{P+P'-2} \quad (3.2.3)$$

$$C_{PP'} = \left(\frac{\hbar^2}{m}\right)^2 \frac{N^2 e^2}{3} \left(R^{P+P'-5}\right) \left[\frac{R}{2\Delta} PP' + \frac{1}{6} (4 - P - P' - 2PP')\right] \quad (3.2.4)$$

They are required to set up the secular equation (3.1.9). The secular equation (3.1.9) can be solved analytically (see appendix). The ensuing spectrum consists of one surface plasmon at  $19.8\text{eV}$  and  $M - 1$  degenerate volume plasmons at  $31.3\text{ eV}$ . It is found that the coupling of translational and compressional dipole modes shift both peaks towards the lower energies, the volume peak by a larger amount than the surface peak.

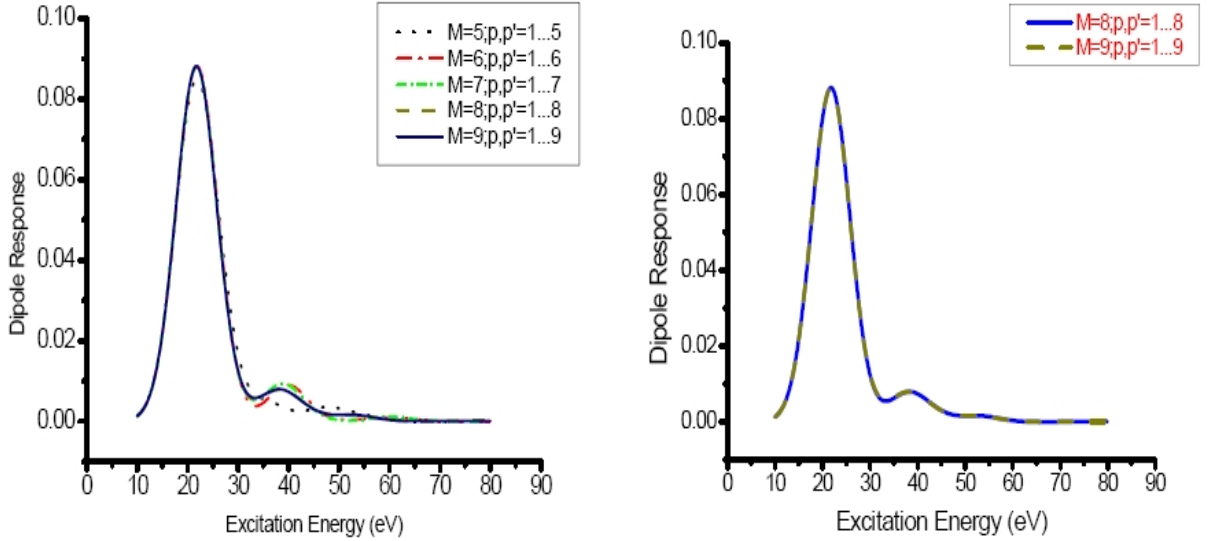


Figure 19: Convergence of the sum-rule weighted dipole response of  $C_{60}$  molecules in the LCA approximation with respect to the number  $M$  of coupled modes with  $p, p' = 1, \dots, M$ .

From the figure 19 it is seen that the convergence is reached at  $M = 8$ . The curves for  $M = 8$  (long dashed) and  $M = 9$  (solid) can not be distinguished. The converged result for  $M = 8$  corresponds to the curve in figure 17. In agreement with experimental data the LCA volume peak is now located at  $38 \text{ eV}$ . The strong collective nature of the dipole plasmon in fullerene  $C_{60}$  molecules suggests the study of higher multipoles as well.

### **3.3 Energies of higher multipole vibrations of fullerenes in a semi-classical approach**

#### **3.3.1 Introduction**

The focus of the present work is an application of the local current approximation (LCA) to the higher collective modes of  $C_{60}$ . In the LCA the ion structure consisting of sixty  $C$  nuclei with their innermost electrons is treated as a fluid while the 240 valence electrons move essentially freely in the potential field created by the constant, positively charged background (jellium model). If stimulated, the valence electrons tend to respond collectively to the external source which leads to collective oscillations. Such collective properties of a many-body system have played an important role in the early years of nuclear physics and are always of utmost interest to physicists because they are often the source of macroscopic effects. The collective dynamic response of delocalized valence electrons in metal clusters to external perturbations has been studied for twenty-five years [68] to [72].

The work of a number of authors studying collective motions in nuclei by a variety of methods has been summarized by Rowe [46]. One of these methods, the liquid drop model, adopts a semi-classical procedure based on the analogy with a fluid droplet. In this system two distinct types of collective vibrations have been investigated: surface vibrations in which the shape is distorted but the volume is kept constant and volume vibrations with fluctuations of the local density. Knowing that the nuclear fluid is nearly incompressible, we expect the volume vibrations to occur at higher energy while the lowest excitations are associated with surface vibrations. For a more detailed study of low-lying excited states of nuclei, the liquid drop model proved to be insufficient. Too few and too widely spaced levels are predicted by this model while the experimental evidence shows a much larger number of energy levels due to single-particle excitations. On the other hand, we notice that the liquid drop model can readily explain the large quadrupole moments and the strong enhancement of  $E_2$  transition rates which are conspicuous features of many nuclei and which are hard to fit into a simple shell theory. In the history of nuclear physics two classical models suggested by Goldhaber and Teller [20] and Steinwedel and Jensen [21] described the physics of giant dipole resonances (GDR) which provide an early explanation of strong collective excitations not only in nuclei but after appropriate modification in general finite fermion systems. Such resonances occur when the system is electromagnetically excited by photons. When a photon hits a nucleus, protons will move due to the electric field thus destroying the optimum mixture of protons and neutrons. After the incident, the proton fluid begins to oscillate against the neutron fluid trying

to reconstitute the local optimum of the mixture.

New techniques to manufacture fullerenes have opened the door to analyze this new and interesting form of carbon. At the end of the 20th century, the electronic structure of solid fullerene has been studied using Auger electron spectroscopy, UV and X-ray photoelectron spectroscopy, UV and X-ray emission and absorption spectroscopy.

For the purpose of the present study the experimental results of [73] are particularly relevant. J. W. Keller and M. A. Coplan investigated the spectrum of the gaseous form of  $C_{60}$  using electron energy loss spectrum (EELS), and compared their results to the spectrum of solid  $C_{60}$  and to optical absorption measurements of solutions of  $C_{60}$ . They presented EELS data of  $C_{60}$  in the gas phase from 1 to 30 eV. Their spectrum is similar to spectra of the solid fullerene, with shifts in the mutually observed bands seen only for the previously identified plasmon features. On the theoretical side, Garibel and Claudia [74], by using a hydrodynamic model, predicted the presence of  $\pi$  plasmons in the range between 6 and 8 eV and  $\sigma$  plasmons near and above 25 eV. Ju [67] et al presented theoretical and experimental electron-energy-loss spectroscopy results illustrating the excitation of collective plasmon states in gas phase fullerene targets. They concluded that states of total angular momentum up to  $L = 8\hbar$  have a collective character. As pointed out in the preceding chapter  $C_{60}$  has a plasmon excitation: 240 delocalized valence electrons oscillating relative to the ion core, produce a giant dipole resonance (GDR) at an excitation energy of 20 eV. S. W. J. Scully et al, [14] from their experimental work at the Lawrence Berkeley

National Laboratory light source, reported the existence of an additional resonance near 40 eV in photoionization of  $C_{60}$  ions. Their experimental data together with time dependent density functional theory (TDLDA) results from the Berlin-Dresden collaboration [63] motivated the present author to attempt an interpretation of higher  $L$  collective excitations with a semi-classical approach (local current approximation or LCA), coupling the surface and volume dipole oscillations in  $C_{60}$  molecules. This semiclassical approach for collective dipole excitations in finite Fermion systems has been applied to metal clusters before [37]. Here it elucidates the coupling of the pure translational mode (surface plasmon) with compressional volume modes. The agreement between the semiclassical LCA and the microscopic TDLDA calculations [63] is surprisingly good.

Volume plasmons can not be excited directly by photoabsorption. Because of the longitudinal nature of volume compression and the transversal nature of light, the photoexcitation of volume plasmons is forbidden in classical electrodynamics. But this is strictly relevant only for extended systems. Recently V. Kresin [75], identified a broad structure which may be interpreted as a volume plasmon absorption peak centered slightly above 4 eV in photodepletion measurements of  $Na_{20}$  and  $Na_{92}$ , thus, revealing the possibility of optical excitation of volume plasmons in a confined metallic system (nanocluster). Recently, Katja et al [76] for the special geometry of a nanoshell, consisting of a dielectric core surrounded by a metallic shell, identified a photoexcited volume plasmon in the spectrum.

The present work is focused on the calculation of the energies of higher multipole

excitations of the 240 valence electrons in  $C_{60}$  molecules and comparison to experimental data [67], [73], using an approach based on a relatively recent paper by Brack et al [61].

### 3.3.2 Theoretical Description

The previous chapters have described the theoretical methods that are employed in this work. We determine multipole excitation energies of  $C_{60}$  using the same electron density which had previously been used to obtain the dipole resonances of  $C_{60}$  [[61] and originated from the Berlin-Dresden collaboration [63]. It is shown in figure 14. This density is matched to an ionic density expressed by step functions

$$\rho_I(r) = \rho_0 [\Theta(R_2 - r) - \Theta(r - R_1)] \quad (3.3.1)$$

where  $R_1 = R - \frac{\Delta}{2}$ ,  $R_2 = R + \frac{\Delta}{2}$  are the inner and outer radii of the shell with the constants given in table 1. The uniform ion density  $\rho_0$  is chosen such that the integrated ion charge is equal but of opposite sign to that of the valence electrons. We hold the ionic charge fixed and unaffected by the oscillations of the valence electrons (jellium model).

The next highest multipole beyond the dipole is the quadrupole mode with excitation energy  $E_3(Q_2)$  defined in section (2.1.7) and excitation operator  $Q_2(\vec{r}) = r^2 Y_{20}$ . The calculation yields its surface plasmon at the energy

$$E_3(Q_2) = \sqrt{\frac{2}{5}} \sqrt{\frac{\hbar^2 N e^2}{m R^2 \Delta}} = 23.4 eV \quad (3.3.2)$$

Extending the operator basis by adding higher basis functions  $Q_L^p(r) = r^P Y_{L0}(\theta)$  with  $L = 2$  and  $P = 3, \dots, M$ , enables the inclusion of compressional modes which couple to the translational surface plasmon. The element of the mass parameter  $B_{PP'}$  and of the restoring force parameter  $C_{PP'}$  for the quadrupole case are given as

$$B_{PP'} = \left( \frac{\hbar^2}{2m} \right) \frac{PP' + 6}{5} N R^{P+P'-2} \quad (3.3.3)$$

$$C_{PP'} = \left( \frac{\hbar^2}{m} \right)^2 \frac{N^2 e^2}{5} \left( R^{P+P'-5} \right) \left[ \frac{R}{2\Delta} PP' + \frac{3}{5} (12 - P - P' - 2PP') \right] \quad (3.3.4)$$

They are the required input to set up the secular equation (3.1.9). Higher multipole modes for  $L = 3$  and 4 have been calculated by the same procedure. The results will be presented and discussed in the next section.

### 3.3.3 Results and Discussion

In the present calculation we have used the electron density given in figure 14. However, we do not distinguish between  $\sigma$ - and  $\pi$ - electrons. Hence, we can not reproduce the low energy structure which would mainly be due to the resonant response from the weakly bound  $\pi$ - electrons. In the formation of the giant resonance peak, however, all electrons are involved and this is the data to which we compare the

present calculations.

### 3.3.4 Giant Monopole Resonances (GMR)

The isoscalar monopole resonance, the so-called breathing mode, has been used extensively as a tool to study the compressibility of nuclear matter. A volume plasmon with multipolarity  $L = 0$  is analogous to the breathing mode vibration, also called as giant monopole resonance. We chose for this mode the monopole operator  $Q_0(r) = r^2 Y_{00}$ , which leads to a good approximation of the breathing mode energy of the system. This monopole operator  $Q_0$  yields a volume plasmon at

$$E_3(Q_0) = \hbar\omega_{vol} = \sqrt{3}\hbar\omega_{Mie} = \sqrt{\frac{\hbar^2 N e^2}{m R^2 \Delta}} = 37 \text{ eV}$$

This breathing mode energy is amazingly in good agreement with the experimentally observed peak. This mode, however, can not be excited directly by external dipole operator because the volume plasmon obtained with the monopole operator does not couple to the electric dipole field. The degree of compressibility of the system can be defined via its breathing mode energy by

$$E_3(Q_0) = \sqrt{\frac{\hbar^2 K_A}{m \langle r^2 \rangle}}$$

where the quantities  $K_A$  and  $\langle r^2 \rangle$  are the "incompressibility parameter" and the mean radius of the system and are model dependent.

### 3.3.5 Giant Quadrupole Resonance (GQR)

We evaluate the sum rules and energies associated with the quadrupole operator

$$Q_2(\vec{r}) = er^2 Y_{20}(\theta)$$

which creates the quadrupole vibrations. The expression (3.3.3) and (3.3.4) are the mass parameter and restoring force parameter (which are the essential ingredients to solve the secular equation ) corresponding to this mode. The energy  $E_3(Q_2)$  corresponding to the surface plasmon vibration is computed at 23.4 eV. Coupling of  $M$  quadrupole operators with  $L = 2$  and  $p = 2, \dots, M$ , one obtains the following spectrum in figure 20.

In agreement with Ju et al [67] measurement, the present LCA calculation shows that the translational quadrupole mode is around 22.5 eV, however, the higher multipole computed in this regime are higher than experimental result. In figure 20 it has been shown that in quadrupole mode for  $M \geq 7$  the spectrum is converged. The converged result for  $M = 7$  corresponds to the dotted curve in figure 20 is given in figure 21 below:

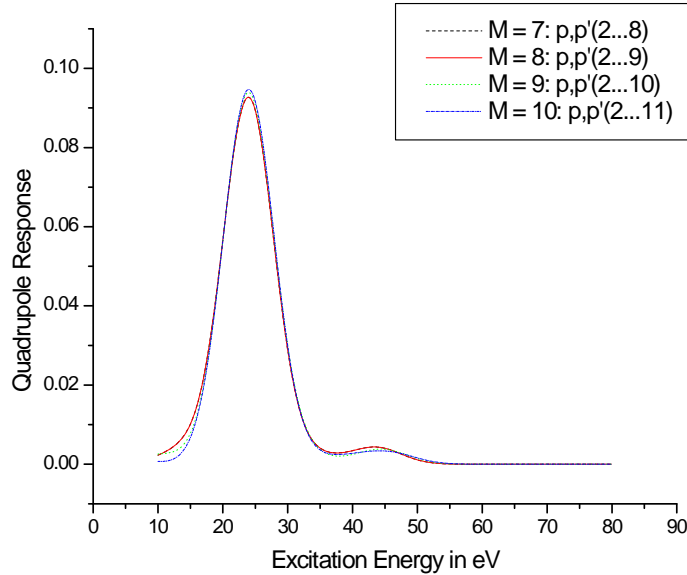


Figure 20: Inclusion of volume changing operators  $Q_L^p$  with  $p \geq 7$  shows the convergence of the sum-rule weighted quadrupole response of  $C_{60}$  molecules in the LCA with respect to the number  $M$  of coupled modes with  $p, p' = 2, \dots, M$ .

### 3.3.6 Giant Octupole Resonance (GOR)

Compared to the rich experimental evidence for the giant dipole and-to a better degree-quadrupole resonances there is little experimental data for the octupole case. The main experimental evidence is provided by the electron-energy-loss data of Bulgac et al [67]. Extending the present approach to  $L = 3$ , we use the operator

$$Q_3(\vec{r}) = er^3 Y_{30}(\theta, \phi)$$

to describe the collective octupole vibration.

Unlike the experimental evidence, our calculations predict compressional modes

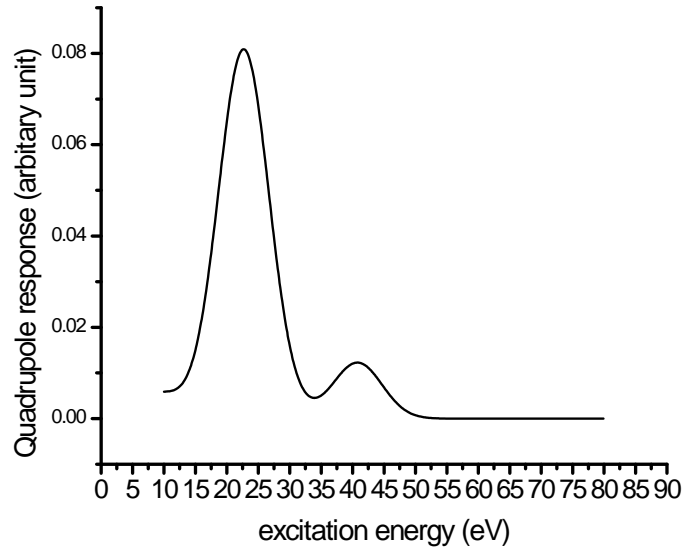


Figure 21: Response of  $C_{60}$  molecules to external stimulation; LCA calculation (Quadrupole mode)

or volume plasmons also for  $L = 2, 3$  and 4 multipoles. If such features are not observable in the experiment, a number of explanations may be given. From the theoretical standpoint, the most likely standpoint is a decrease in collectivity with increasing angular momentum of the multipole vibrations. The present form of the LCA model does not provide an option to modify collectivity by distributing the oscillator strength over a wider range of energies. But there is indirect experimental evidence to support the existence of volume plasmon. The coupling of surface and volume plasmons is the cause of a shift of both peaks to lower energy values: more for the surface modes than for compressional modes. This has been pointed out for the dipole case [61] before and has been found again here for  $L = 2, 3,$  and 4. The coupling shifted surface peaks are in better agreement with experimental data than

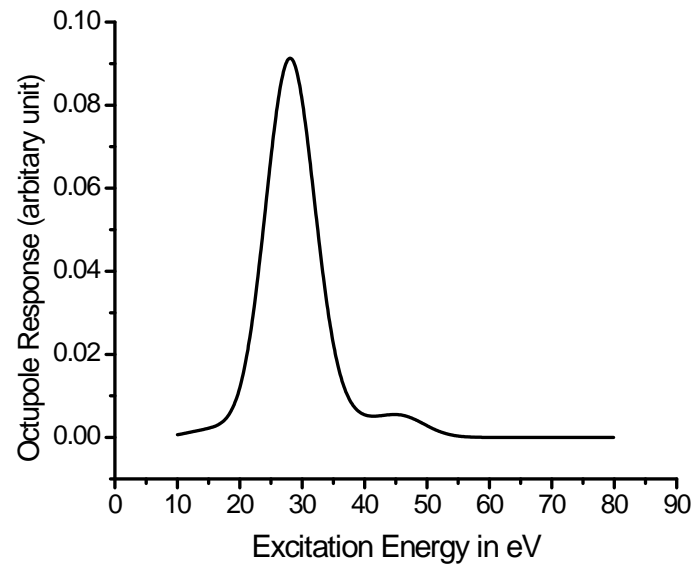


Figure 22: Response of  $C_{60}$  molecules to external stimulation; LCA calculation (Octupole mode)

the unshifted pure surface plasmons. The obtained agreement is excellent for the dipole case  $L = 1$ , acceptable for  $L = 2$  and deteriorates with increasing angular momentum.

Multipole Order	Operator	Pure Surface Plasmon	Coupling shifted Surface Plasmon	Experiment	Coupling shifted Volume Plasmon
$L = 1$	$r^1 Y_{20}$	$22.1 \text{ eV}^{(a)}$	$21.4 \text{ eV}^{(a)}$	$21.4 \text{ eV}^{(c)}$	$37 \text{ eV}^{(a)}$
$L = 2$	$r^2 Y_{20}$	$25 \text{ eV}^{(a)}$	$22.5 \text{ eV}^{(a)}$	$21 \text{ eV}^{(b)}$	$41 \text{ eV}^{(a)}$
$L = 3$	$r^3 Y_{30}$	$29 \text{ eV}^{(a)}$	$26 \text{ eV}^{(a)}$	$21.5 \text{ eV}^{(b)}$	$42 \text{ eV}^{(a)}$
$L = 4$	$r^4 Y_{40}$	$32 \text{ eV}^{(a)}$	$28.5 \text{ eV}^{(a)}$	$22 \text{ eV}^{(b)}$	$42 \text{ eV}^{(a)}$

Table 3: The LCA multipole response of fullerene molecules

$a$  : Present LCA calculation

$b$  : Experimental data [67]

$c$  : Experimental data [14]

The results in column three represent the energies in  $eV$  of the surface modes calculated with the operators given in column two. Columns four and five are obtained by augmenting the operators with the volume changing contributions discussed in section 3: This change affects the appearance of the volume plasmon and also shifts both peaks to lower energies. The volume plasmon has experimentally been verified for the dipole case but so far not for higher multipoles. Compressional effects seem to be less pronounced both in our calculations and obviously also in experimental work, which so far, not reported compressional peaks. Direct comparison of our results to experimental data by Bulgac [67] is therefore restricted to the results given in columns four and five of table 3.

## 4 Chapter

### 4.1 Summary and Conclusions

Fullerenes are one of the finite Fermion systems, that have drawn an extensive scientific interest since its discovery due to hand in hand progress in theoretical and experimental techniques and due to technological prospects. This work investigated the collective dynamic response of the 240 delocalized valence electrons of the fullerene  $C_{60}$  molecules to an external stimulation such as electromagnetic radiation or scattering of charged particle, using the local current approximation (LCA), a semiclassical approach which is based on a general variational principle.

Optical response of fullerene  $C_{60}$  molecules were calculated from a collective model that describes the density dynamics of electronic excitations by scaling transformation. Our model is best illustrated by quantum mechanical equation of motion for excitation operators by a variational principle. For the finite basis set, eigenvalue equations for the displacement fields associated with electronic excitations were derived from variational principle and solved to get the excitation energy. This approach, which had previously been applied to study the collective excitation of metal clusters [61], has here been applied to compute the optical response of the fullerene  $C_{60}$  molecules.

A giant surface plasmon resonance near  $22\text{ eV}$  is prominent in absolute photoionization measurement, which contain an additional broad feature near  $38 \pm 2\text{ eV}$  that is indicative of a higher order plasmon oscillation, also called as volume plasmon.

Using the jellium model, TDLDA calculations reproduce this result. In the LCA regime we have obtained the similar features as the TDLDA, using the same jellium model. Since the jellium model neglect the ionic structure, the collective peaks in both TDLDA and LCA calculations appear at too low energy. Therefore TDLDA curve has been artificially blue shifted by 5.5 eV and have done the same with our LCA calculations.

We have also calculated the multipole excitation energies of the  $C_{60}$  molecules using the same jellium model in LCA regime. The excitation energies of  $C_{60}$  for increasing order of angular momentum up to  $L = 4$  have been calculated, and it has been found that the coupled surface plasmon for the higher multipole modes stretch out in 22 – 28 eV whereas the coupled volume plasmons were found in 40 – 42 eV. These multipole energies computed in LCA regime are higher than the experimental results. The volume plasmon which has experimentally been verified for the dipole case but so far not for higher multipoles. Compressional effects are less pronounced in our calculations and obviously also in experimental work which so far has not reported these features.

In the present calculation we have used the electron density obtained from TDLDA calculations performed and generously supplied to us by authors [63]. This data does not distinguish the contributions from  $\pi$ - and  $\sigma$ - electrons separately. This fact makes it impossible to reproduce the prominent  $\pi$ - electron resonance seen in some experiments [67], but it enables us to compare our LCA results to their TDLDA results on the same footing (i. e. same electron density and same ion potential). The

excellent agreement between the two theoretical findings and the closeness of both to the experimental findings (Fig. 17) lend strong support to the interpretation as collective dipole oscillations. We notice, however, that the experimental photoexcitation data starts at an energy which is higher than the response of the  $\pi$ - electrons alone which has been determined at 6 eV by inelastic electron excitation by a different experimental group.

The coupled oscillator system addressed in appendix C is a first attempt to reproduce the distinct responses of the  $\pi$ - and  $\sigma$ - electron systems in a classical mechanical model. The translation of the mechanical findings into the framework of the LCA approach is possible and presently being studied by us. The major hurdle to be overcome in this task is the calculation of the electron orbitals for the high angular momentum states. For  $C_{60}$ , orbitals up to an angular momentum quantum number  $l = 9$  are needed in Hartree-Fock approximation or, preferably, in TDLDA to make the set of electron density consistent.

## 5 Appendices

### 5.1 Appendix A :

#### 5.1.1 Evaluation of equations (2.10.2) and (2.10.3)

To compute the commutators in equations (2.10.2) and (2.10.3) and consequently equation (3.1.10) and (3.1.11) we start with the operators

$$Q_L^p = r^p Y_{L0}(\theta)$$

Assume that for a given hamiltonian with kinetic energy  $\hat{T}$  and potential energy  $\hat{V}$

$$\hat{H} = \hat{T} + \hat{V}$$

one has scaling operator

$$S = [\hat{H}, \hat{Q}_L^p] = [\hat{T}, \hat{Q}_L^p]$$

For the local operator  $\hat{Q}$  which commutes with the potential energy  $V$  in the total hamiltonian  $\hat{H} = \hat{T} + \hat{V}$  the scaling operator  $\hat{S}$  and the moments  $m_1$  and  $m_3$  have a simple physical meaning. We define the scaling operator  $S$  by

$$S_L^p = [\hat{H}, \hat{Q}_L^p] = [\hat{T}, \hat{Q}_L^p] = \frac{1}{2} (\nabla \cdot \mathbf{u}_L^p) + \mathbf{u}_L^p \cdot \nabla \quad (\text{A1})$$

where  $\mathbf{u}$  is a displacement field given by

$$\mathbf{u}_L^p(\mathbf{r}) = -\frac{\hbar^2}{m} \nabla Q_L^p(\mathbf{r})$$

The operator  $\hat{S}$  creates a scaled state by means of a unitary transformation

$$|\alpha\rangle = e^{-\alpha S_L^p} |0\rangle$$

where the real variable  $\alpha$  is scaling parameter and is also understood as a collective variable  $\alpha(t)$ . One write the time dependent one body density

$$\rho(\mathbf{r}, t) = \rho(\mathbf{r}, \alpha(t)) = \sum_{i=1}^A |\psi_i(\mathbf{r}, \alpha)|^2 = e^{-\alpha((\mathbf{r} \cdot \mathbf{u}) + \mathbf{u} \cdot \mathbf{r})} \rho(\mathbf{r})$$

Now the velocity field

$$\mathbf{v}(\mathbf{r}, t) = \dot{\alpha}(t) \mathbf{u}(\mathbf{r})$$

and the local currents

$$\mathbf{j}_\alpha(\mathbf{r}, t) = \rho_\alpha(\mathbf{r}, t) \mathbf{v}(\mathbf{r}, t)$$

which satisfies the continuity equation

$$\frac{\partial}{\partial t} \rho_\alpha(\mathbf{r}, t) + \nabla \cdot \mathbf{j}_\alpha(\mathbf{r}, t) = 0$$

and that

$$B_{PP'} = \frac{m}{2\hbar^2} \int \vec{u}_L^P(\vec{r}) \cdot \vec{u}_L^{P'}(\vec{r}) \rho(\vec{r}) d^3r$$

with

$$\vec{u}_L^P(\vec{r}) = -\frac{\hbar^2}{m} \nabla Q_L^P(\vec{r}), Q_L^P(\vec{r}) = r^P Y_{L,0}(\theta, \phi)$$

$$B_{PP'} = \frac{\hbar^2}{2m} \frac{PP' + L(L+1)}{2L+1} (4\pi) \int_0^\infty r^{P+P'} \rho(r) dr$$

$$\text{or } B_{PP'} = \frac{\hbar^2}{2m} \frac{PP' + L(L+1)}{2L+1} (4\pi) \int_{R_1}^{R_2} r^{P+P'} \frac{N}{V} dr$$

$$\text{or } B_{PP'} = \frac{\hbar^2}{2m} \frac{PP' + L(L+1)}{2L+1} \frac{4\pi N}{V} \int_{R_1}^{R_2} r^{P+P'} dr$$

$$\text{or } B_{PP'} = \frac{\hbar^2}{2m} \frac{PP' + L(L+1)}{2L+1} \frac{4\pi N}{\frac{4\pi}{3}(R_2^3 - R_1^3)} \int_{R_1}^{R_2} r^{P+P'} dr$$

where  $R_1 = R - \frac{\Delta}{2}$  and  $R_2 = R + \frac{\Delta}{2}$

$$\text{or } B_{PP'} = \frac{\hbar^2}{2m} \frac{PP' + L(L+1)}{2L+1} \frac{3N}{P+P'+1} \frac{(R + \frac{\Delta}{2})^{P+P'+1} - (R - \frac{\Delta}{2})^{P+P'+1}}{(R + \frac{\Delta}{2})^3 - (R - \frac{\Delta}{2})^3}$$

$$\text{or } B_{PP'} = \frac{\hbar^2}{2m} \frac{PP' + L(L+1)}{2L+1} \frac{3N}{P+P'+1} \frac{[R^{P+P'+1} \left\{ (1 + \frac{\Delta}{2R})^{P+P'+1} - (1 - \frac{\Delta}{2R})^{P+P'+1} \right\}]}{R^3 \left[ (1 + \frac{\Delta}{2R})^3 - (1 - \frac{\Delta}{2R})^3 \right]}$$

Using Binomial theorem

$$(1+x)^n = 1 + nx + \dots\dots\dots$$

$$\left(1 + \frac{\Delta}{2R}\right)^3 - \left(1 - \frac{\Delta}{2R}\right)^3 = 3\frac{\Delta}{R}$$

$$\left(1 + \frac{\Delta}{2R}\right)^{P+P'+1} - \left(1 - \frac{\Delta}{2R}\right)^{P+P'+1} = (P+P'+1)\frac{\Delta}{R}$$

$$\therefore B_{PP'} = \left(\frac{\hbar^2}{2m}\right) \frac{PP'+L(L+1)}{2L+1} NR^{(P+P'-2)}$$

The restoring force parameter defined in equation (12) can be rewritten as

$$\begin{aligned} C_{pp'} &= \frac{1}{2} \langle 0 | [S_L^p, [S_L^{p'}, \hat{H}]] | 0 \rangle \\ &= \frac{d^2}{d\alpha d\alpha'} \left[ \langle 0 | e^{\alpha S_L^p} \hat{H} e^{-\alpha' S_L^{p'}} | 0 \rangle \right]_{\alpha=\alpha'=0} \\ &= \frac{d^2}{d\alpha d\alpha'} \left[ \langle \alpha | \hat{H} | \alpha' \rangle \right]_{\alpha=\alpha'=0} \end{aligned} \quad (\text{A2})$$

where

$$|\alpha\rangle = e^{-\alpha S_L^p} |0\rangle$$

is the scaled ground state. Now one can write

$$C_{pp'} = C_{pp'}^{kin} + C_{pp'}^{xc} + C_{pp'}^{Coul} + C_{pp'}^{VI}$$

Note that  $S_L^p$  and  $S_L^{p'}$  even do not commute,  $C_{pp'}$  in equation (A2) would be symmetric as long as  $|0\rangle$  is eigenstate of  $\hat{H}$ . The kinetic energy term for  $L = 1$  is calculated analytically (please see [81] and for  $L > 1$  involves complicated angular momentum algebra and is very cumbersome to evaluate in general. It has been evaluated in the local density approximation, which for the kinetic energy means using the Thomas-fermi functional (please see [37] for detail). The exchange-correlation contribution has been evaluated in the local density approximation. The following formula is used for any part of energy that is just a spatial integral over a function  $f$  of the density  $\rho(r)$ . The energy functional  $E_f$  is given by

$$E_f = E_f[\rho] = \int f(\rho(r)) d^3r$$

Then the symmetrized contribution to  $E_f$  (A2) is found to be

$$C_{PP'}^f = \frac{1}{2} \left( \frac{\hbar^2}{m} \right)^2 \frac{4\pi}{(2L+1)} \int_0^\infty r^{p+p'-2} \times \left[ \begin{aligned} &(p+p'-1) \{p[p'(p'+1) - L(L+1)] + p'[p(p+1) - L(L+1)]\} \left[ f(\rho) - \rho \frac{df(\rho)}{d\rho} \right] \\ &+ 2[p(p+1) - L(L+1)] [p'(p'+1) - L(L+1)] \rho^2 \frac{d^2f(\rho)}{d\rho^2} \end{aligned} \right] dr \quad (\text{A3})$$

The symmetrized Hartree-Coulomb contribution to  $C_{PP'}^{coul}$  is

$$C_{PP}^{coul} = \left( \frac{\hbar^2}{m} \right)^2 \frac{(4\pi e)^2}{2(2L+1)} \frac{L(L+1)}{(2L+1)} \int_0^\infty \rho(r) \times \quad (A4)$$

$$\left[ \begin{array}{l} \frac{1}{2} (L-P)(P+L+1) r^{P-L-1} \int_0^r r'^{L+P} \rho(r') dr' \\ + (L-P)(P+L+1) r^{P-L-1} \int_0^r r'^{L+P} \rho(r') dr \end{array} \right] dr$$

$$C_{PP}^{coul} = \left( \frac{\hbar^2}{m} \right)^2 \frac{(4\pi e)^2}{2(2L+1)} \frac{L(L+1)}{(2L+1)} \frac{N}{4\pi R^2 \Delta} \int_0^\infty \rho(r) \left[ \begin{array}{l} (L-P) R^{P+P} (P+L+1) \frac{\Delta}{R} \\ + (L-P) R^{P+P} (P+L+1) \frac{\Delta}{R} \end{array} \right] dr$$

$$C_{PP}^{coul} = \left( \frac{\hbar^2}{m} \right)^2 \frac{(4\pi e)^2}{2(2L+1)} \frac{L(L+1)}{(2L+1)} \frac{N}{4\pi R^2 \Delta} \int_{R_1}^{R_2} \rho(r) \left[ \begin{array}{l} (L-P)(P+L+1) \\ + (L-P)(P+L+1) \end{array} \right] \frac{\Delta}{R} R^{P+P} dr$$

$$C_{PP}^{coul} = \frac{1}{2} \left( \frac{\hbar^2}{m} \right)^2 \frac{N^2 e^2}{(2L+1)} \frac{L(L+1)}{(2L+1)} \frac{N^2}{4\pi R^2 \Delta} (2L^2 + 2L - P - P' - 2PP') R^{P+P-5}$$

The contribution from any external spherical potential  $V_I(r)$  is

$$C_{PP}^{V_I} = \left( \frac{\hbar^2}{2m} \right)^2 \frac{4\pi}{(2L+1)} \int_0^\infty V_I(r) r^{p+p'-2} \times \quad (A5)$$

$$\left[ \begin{aligned} & (p+p'-1) [(p+p'+2)pp' - (p+p')L(L+1)] \rho(r) \\ & + [(3p+3p'-2)pp' - (p+p')L(L+1)] r \frac{d\rho(r)}{dr} + 2r^2 pp' \frac{d^2\rho(r)}{dr^2} \end{aligned} \right] dr$$

After doing little algebra, we get

$$C_{PP}^{V_I} = \left( \frac{\hbar^2}{2m} \right)^2 \frac{4\pi}{(2L+1)} 2PP' \int_{R_1}^{R_2} \nabla^2 V_I(r) r^{P+P'} \rho(r) dr$$

$$C_{PP}^{V_I} = \left( \frac{\hbar^2}{2m} \right)^2 \frac{4\pi}{(2L+1)} 2PP' (4\pi e^2) \int_{R_1}^{R_2} \rho_{I0}(r) r^{P+P'} \rho(r) dr$$

$$C_{PP}^{V_I} = \left( \frac{\hbar^2}{2m} \right)^2 \frac{4\pi}{(2L+1)} 2PP' (4\pi e^2) \int_{R_1}^{R_2} \rho_0 [\Theta(R_2 - r) - \Theta(R_1 - r)] r^{P+P'} \rho(r) dr$$

$$C_{PP}^{V_I} = \left( \frac{\hbar^2}{2m} \right)^2 \frac{4\pi}{(2L+1)} \frac{4\pi e^2 N^2}{(16\pi^2 R^4 \Delta^2)} \frac{2PP'}{(P+P'+1)} \left( R_2^{(P+P'+1)} - R_1^{(P+P'+1)} \right)$$

$$C_{PP}^{V_I} = \left( \frac{\hbar^2}{m} \right)^2 \frac{N^2 e^2}{(2L+1)} \frac{R}{2\Delta} PP' \left[ R^{(P+P'-5)} \right]$$

$$C_{PP'} = C_{PP'}^{coul} + C_{PP'}^{V_I}$$

$$C_{PP'} = \left(\frac{\hbar^2}{m}\right)^2 \frac{N^2 e^2}{(2L+1)} \left(R^{(P+P'-5)}\right) \left[ \frac{R}{2\Delta} P P' + \frac{L(L+1)}{2(2L+1)} (2L^2 + 2L - P - P' - 2PP') \right]$$

For quadrupole motion,  $L = 2$  and  $P, P' = 2$ , then

$$C_{PP'} = \left(\frac{\hbar^2}{m}\right)^2 \frac{N^2 e^2}{5} \frac{2}{\Delta}$$

$$B_{PP'} = \left(\frac{\hbar^2}{m}\right) N R^2$$

The energy  $E_3$  discussed in section three is written as

$$E_3 [\hat{Q}] = \sqrt{\frac{m_3 [\hat{Q}]}{m_1 [\hat{Q}]}} = \sqrt{\frac{C_{PP'}}{B_{PP'}}}$$

$$E_3 (Q_2) = \sqrt{\frac{2}{5}} \sqrt{\frac{\hbar^2 N e^2}{m R^2 \Delta}}$$

If we set  $p = p' = L$ , and using equation (A3), (A4), and (A5) we can recover the following equations:

$$m_1 (Q_L) = \frac{\hbar^2 L}{m} \frac{1}{2} \int r^{2L-2} \rho(r) d^3 r$$

$$m_3^{Coul} = - \left[ \frac{\hbar^2}{m} \right]^2 \frac{L^2 (L-1)}{2L+1} (4\pi e)^2 \times \int_0^\infty r^{2L-3} \rho(r) dr \int_0^r (r')^2 \rho(r') dr'$$

$$m_3^{VI} = \left[ \frac{\hbar^2}{m} \right]^2 \frac{L^2}{2(2L+1)} \times \int_0^\infty V_I(r) r^{2L-4} [r^2 \rho''(r) + 2rL\rho'(r)] d^3r$$

where  $\rho'(r)$  and  $\rho''(r)$  are radial derivatives. Note that the exchange-correlation energy in LDA, like any part of the total energy which is only a function of  $\rho(r)$ , does not contribute to  $m_3(Q_L)$  [81]

### 5.1.2 Local density approximation

Local density approximation (LDA) is the beautiful tool to compute the exchange-correlation energy when dealing with the energy functional of the finite fermion system. The LDA works well for the system in which the electron density does not vary too rapidly. More details about the LDA is collected in references [35], [89], [90], [91] and [92]. In this approximation the exchange correlation energy is written as

$$E_{xc} = \int d^3r \rho(r) \varepsilon_{xc}[\rho(r)]$$

The exchange energy part of the LDA as derived by Dirac is given

$$E_x = -\frac{3}{4} \left[ \frac{3}{\pi} \right]^{\frac{1}{3}} \varepsilon^2 \int [\rho(r)]^{\frac{4}{3}} d^3r$$

In the present work to calculate the exchange-correlation energy we have used the following correlation energy;

$$\epsilon_c^W = -\frac{0.88}{r_s(\rho) + 7.8}$$

where  $r_s$  is Wigner Seitz radius. This is the most commonly used correlation energy functional in cluster physics and is derived by Wigner. Similarly Gunnarsson and Lundqvist also developed a correlation energy functional which is given by

$$\epsilon_c^{GL} = -0.0666 \left[ (1 + X^3) \log \left[ 1 + \frac{1}{X} \right] + \frac{1}{2}X - X^2 - \frac{1}{3} \right]$$

where

$$X = \frac{r_s(\rho)}{11.4}$$

In the density functional theory the LDA approach has turned out to be very successful. In some system, however, it leads to noticeable deviations.

## 5.2 Appendix B :

### 5.2.1 solution of the secular equation

Here the general solution of the secular equation (3.1.9) presented in detail;

$$\det |C_{pp'} - (\hbar\omega)^2 B_{pp'}| = f(L) \det |A_{pp'}| = 0, \quad (p, p' = 1, 2, \dots, M)$$

where  $f(L)$  is a factor independent of  $p, p'$ , and the matrix  $A_{pp'}$  is given by

$$A_{pp'} = \frac{(2L+1)pp' + L(L+1)(2l-p-p') - \lambda(2L+1)[pp' + L(L+1)]}{(1+p+p')}$$

where the eigenvalue  $\lambda$  is the squared ratio of frequencies

$$\lambda = \left( \frac{\omega}{\omega_{vol}} \right)^2$$

$$A_{pp'} = \frac{\{(2L+1)pp' + 2L \cdot L(L+1) - L(L+1)(p+p') - \lambda(2L+1)[pp' + L(L+1)]\}}{(1+p+p')}$$

$$A_{pp'} = \frac{\{(2L+1)pp' + 2L \cdot L(L+1) + L(L+1) - L(L+1) - L(L+1)(p+p') - \lambda(2L+1)[pp' + L(L+1)]\}}{(1+p+p')}$$

$$A_{pp'} = \frac{(2L+1)pp' + L(L+1)(2L+1) - L(L+1)(1+p+p') - \lambda(2L+1)[pp' + L(L+1)]}{(1+p+p')}$$

$$A_{pp'} = \frac{(2L+1)[pp' + L(L+1)] - L(L+1)(1+p+p') - \lambda(2L+1)[pp' + L(L+1)]}{(1+p+p')}$$

$$A_{pp'} = \frac{(2L+1)[pp' + L(L+1)](1-\lambda) - L(L+1)(1+p+p')}{(1+p+p')}$$

$$A_{pp'} = \frac{(2L+1) \left\{ [pp' + L(L+1)](1-\lambda) - \frac{L(L+1)}{2L+1}(1+p+p') \right\}}{(1+p+p')}$$

$$A_{pp'} = \left[ \frac{(pp' + F)(1-\lambda)}{(1+p+p')} - G \right]$$

where  $F = L(L + 1)$  and  $G = \frac{L(L+1)}{2L+1}$

$$\det |A_{pp'}| = (2L + 1)^M \det |D_{pp'}| = 0$$

where  $D_{pp'} = \frac{(1-\lambda)(pp'+F)}{(1+p+p')} - G$

Now  $L = 0$ , then  $F = G = 0$  and the characteristic equation becomes

$$\det|(1 - \lambda) pp' / (1 + p + p')| = (1 - \lambda)^M \det|pp' / (1 + p + p')| = 0$$

since for any  $p, p' > 0$  the determinant on the r.h.s above is never zero, we get  $M$  degenerate solutions with eigenvalue  $\lambda = 1$ .

$$\begin{aligned} \det |A_{pp'}| &= (2 \cdot 0 + 1)^M \det|(1 - \lambda) pp' / (1 + p + p')| \\ &= (1 - \lambda) \det|(1 - \lambda) / (1 + p + p')| = 0 \end{aligned}$$

$L > 0$  : In this case  $F$  and  $G$  are non-zero and the matrix  $D_{pp'}$  has the form

$$D_{pp'} = \begin{pmatrix} \frac{(1-\lambda)(1+F)}{3} - G & \frac{(1-\lambda)(2+F)}{4} - G & \dots & \\ \frac{(1-\lambda)(2+F)}{4} - G & \frac{(1-\lambda)(4+F)}{5} - G & \dots & \\ \frac{(1-\lambda)(3+F)}{5} - G & \frac{(1-\lambda)(6+F)}{6} - G & \dots & \\ \dots & \dots & \dots & \dots \end{pmatrix}$$

Notice that in each element, the first term contains the factor  $(1 - \lambda)$  and the second term is the constant  $-G$ . we now replace the first row by the difference between the first and second rows, the second by the difference between the second and third, and so on, until we reach the last row in which we do not change anything. The determinant, whose value is not altered by these manipulations, then becomes

$$\det |D_{pp'}| = \begin{vmatrix} (1 - \lambda) E_{11} & (1 - \lambda) E_{12} & \dots & (1 - \lambda) E_{1M} \\ (1 - \lambda) E_{21} & (1 - \lambda) E_{22} & \dots & (1 - \lambda) E_{2M} \\ \dots & \dots & \dots & \dots \\ (1 - \lambda) E_{M1} - G & (1 - \lambda) E_{M2} - G & \dots & (1 - \lambda) E_{MM} - G \end{vmatrix}$$

where the  $E_{pp'}$  are linear expressions in the constant F. Only in the last row the additive constant  $-G$  remains, while all other elements now are proportional to  $(1 - \lambda)$ . The characteristic equation therefore becomes

$$\det |D_{pp'}| = (1 - \lambda)^{(M-1)} \det |\tilde{E}_{pp'}| = 0$$

where  $\tilde{E}_{pp'}$  is the remaining matrix after removing the factor  $(1 - \lambda)$  from the first  $M - 1$  rows in above matrix, its determinant is linear in  $\lambda$ .

## 5.3 Appendix C

### 5.3.1 Coupled Oscillator System as a Mechanical Analogy to the Responses of $\pi$ - and $\sigma$ - Electrons.

The purpose of this appendix is to set up the  $\pi$  and  $\sigma$  electrons of fullerene molecules as individual classical oscillator. In our computation of semiclassical model we did not distinguish the  $\pi$  and  $\sigma$  electron due to the lack of  $\pi$  electron density.

### 5.3.2 Introduction

There are several forms of natural carbon, graphite and diamond being the most familiar. Kroto et al [5] discovery established that there is a third form of carbon: the fullerene  $C_{60}$ . Since its discovery in 1985, there have been both theoretical and experimental efforts to investigate the behavior of  $C_{60}$ . One of the simplest theoretical models of  $C_{60}$  is the jellium model. In the jellium model, the 240 valence electrons of  $C_{60}$  are treated as free electrons, moving in a shell of uniform positive charge representing the field of the positive carbon ions, which form the fullerene's cage-like structure.

We have calculated the photo-excitation cross-section of  $C_{60}$ , within the framework of the jellium model, using the local current approximation (LCA) calculations [93]. These calculations produce results that resemble those of the time-dependent local density approximation (TDLDA). Both methods suggest that experimentally observed features in the photo-excitation cross-section of  $C_{60}$ , correspond to collective oscillations of the 240 valence electrons, relative to the background of positive carbon ions.

A mass attached to a spring executes simple harmonic motion. How does the motion of this simple harmonic oscillator change when coupled, by a spring, to another simple harmonic oscillator? Consider two linear oscillators joined by a spring, if initially one oscillator is placed in motion, the second oscillator eventually begins to move as well. The connecting spring serves to transfer energy from the motion of the first oscillator into motion of the second. Usually, the energy of the system oscillates

back and forth between the two oscillators. The analysis of such a system of coupled oscillators is often used as an introduction to the concepts of normal coordinates and normal modes of vibrations. For the normal modes of vibration, the motion is simple harmonic. However, the general behavior of coupled harmonic oscillators is not necessarily simple harmonic motion.

The fullerene molecule is an allotropic form of carbon, with remarkable properties. The molecule is an empty, closed cage comprised entirely of  $sp^2$ -hybridized carbon atoms arranged in regular patterns of hexagons and pentagons, twelve pentagons and twenty hexagons. There are 240 valence electrons in  $C_{60}$  molecules of which 60 electrons are the weakly bound  $\pi$  electrons and 180 electrons are the more tightly bound  $\sigma$  electrons. The total number of bonds in a  $C_n$  fullerene is  $\frac{3n}{2}$ . In  $C_{60}$ , the length of the bond between two hexagons is  $1.38 \text{ \AA}$ , whereas the bond between a pentagon and a hexagon is  $1.45 \text{ \AA}$  [7]. To understand the electronic properties and interatomic bonding of fullerene molecules, it is useful to consider the electronic eigenstates corresponding to the  $\pi$  and  $\sigma$  electron orbitals. As pointed out in reference [94], states without nodes in the radial direction, correspond to the  $\sigma$  orbitals and states with one node in the radial direction, correspond to  $\pi$  orbitals. Orbitals with a radial node extend further into the radial direction and thus are less bound than nodeless orbitals. More electronic properties of  $C_{60}$  molecule are given in references [60], to [11]. The ground state configuration for the neutral  $C_{60}$  fullerene molecules given by

Polozkov et al [78]

$$\underbrace{1s^2 2p^6 3d^{10} 4f^{14} 5g^{18} 6h^{22} 7i^{26} 8k^{30} 9l^{34} 10m^{18}}_{\text{without node}} \underbrace{2s^2 3p^6 4d^{10} 5f^{14} 6g^{18} 7h^{10}}_{\text{with one node}}$$

Fullerene molecules have a symmetric structure and bridge the gap between the free molecules and solids. As a result, fullerenes can possess chemical and physical properties of both solids and free molecules. Within the simplest approximation, the jellium model, the 240 valence electrons in a  $C_{60}$  molecule are treated as free electrons moving in the field of the positive carbon ions of the molecule. These free electrons respond collectively to electromagnetic radiation of varying frequencies. The resonant collective oscillation of the free electrons is known as plasma oscillation or plasmon.

Experimentally,  $C_{60}$  shows two predominant resonances: one at  $5eV$  and another around  $20eV$  [14] of energy. Theoretically, these resonances are interpreted as dipole vibration modes [61]. Garibel and Claudia [74], used the so-called hydrodynamic model, to predict the presence of a  $\pi$  plasmon in the 6 to 8  $eV$  energy range and  $\sigma$  plasmon near and above 25  $eV$ . In their photoexcitation study of  $C_{60}$  ions Scully et al, report the existence of an additional photoionization resonance near 40  $eV$  [14] with less prominent features. These features have been named "volume plasmon" because they are caused by density changing terms in the system's Hamiltonian. We do not attempt to include density changing terms here, but rather study the analogy

of the oscillator model to just the  $\pi$ - and  $\sigma$ -resonances.

Plasma oscillations play an important role in the optical properties of conductors and semi-conductor materials. These materials are transparent to electromagnetic waves with a frequency above the plasma frequency and opaque to waves with a frequency below the plasma frequency. For electromagnetic waves with frequency above the plasma frequency, the electrons in the material respond too slowly to cancel the rapidly oscillating electric field completely, and the field penetrates the material, i.e. transmitted. Light of frequency below the plasma frequency is reflected, the electrons in the metal can respond fast enough to cancel the incident electric field. In metal clusters, the plasma frequency happens to be in the ultraviolet region making them reflective in the visible range. The brilliant colors in medieval stained glass windows results from the resonant light scattering from gold and silver particles of different size that were added to the glass. Metallic clusters with electronic interband transitions in the visible range absorb specific colors of light, yielding distinct colors in reflection.

Although the density changing oscillation (volume plasmon) does not lead to an experimentally pronounced peak, its presence is felt indirectly because it is responsible for the shift of the surface plasmon to lower energies [14] [75]. Without the interaction of the two modes, i.e. surface and volume plasmons, the predicted resonances would both occur at higher energy than the experiment determines. Volume plasmons become less and less relevant for higher multipole excitations but their presence is likewise felt indirectly by shifting of the corresponding surface modes to lower

energies.

### 5.3.3 Theory

Consider the system shown in figure 23. The system consists of two different masses,  $m_1$  (corresponding to mass of 180 electrons) and  $m_2$  (mass of 60 electrons) connected to each other and to two fixed points by springs, of which the outer ones have the spring constants  $k_1$  and  $k_2$  as show in figure 23. The central spring with constant  $k$  weakly couples the two oscillators if we choose  $k \ll k_1, k_2$ . When there is no coupling between the masses  $k = 0$ , each mass oscillates harmonically with its proper frequency  $\omega_i = \sqrt{k_i/m_i}$ , independently of the other. The spring forces are the only forces acting in this idealized one-dimensional system. Later we will introduce damping as well as a harmonic driving force. The motion at any given time is completely specified by two coordinates, the displacements  $x_1(t)$  and  $x_2(t)$  from the equilibrium position of each mass. The springs exert zero resulting force when the system is in equilibrium [79].

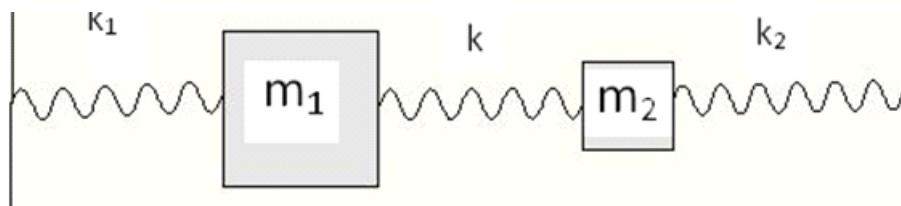


Figure 23: Coupled system

We analyze the system in the framework of forced oscillations and resonances. In

the absence of damping, the equations of motion of the system can be written as,

$$F_j = m_j \frac{d^2 x_j}{dt^2} = - \sum_k k_{jk} x_k \text{ for } j = 1, 2 \quad (4.1)$$

It is useful to rewrite expression (4.1) in matrix notation

$$\frac{d^2 X}{dt^2} = -M^{-1} K X \quad (4.2)$$

where

$$X = \begin{bmatrix} x_1 \\ x_2 \end{bmatrix}, \quad K = \begin{bmatrix} k_{11} & k_{12} \\ k_{21} & k_{22} \end{bmatrix}, \quad \text{and} \quad M = \begin{bmatrix} m_1 & 0 \\ 0 & m_2 \end{bmatrix}, \quad I = \begin{bmatrix} 1 & 0 \\ 0 & 1 \end{bmatrix}$$

$X$  is a column vector, whose row is the displacement  $x_i$ .  $K$  is the "K-matrix" and  $M$  is the "mass matrix".

Assuming small displacements the springs obey Hooke's law and thus exert a linear restoring force on the masses given by

$$F = -k(x - x_0)$$

To set up the value of the constant  $k_{jk}$  one displaces mass  $m_2$  while keeping mass  $m_1$  fixed in its equilibrium position. For the small displacement of mass, there will be the restoring force  $kx_2$  on mass  $m_1$  and  $-kx_2$  on mass  $m_2$ . Here we have presented

only a few important steps. From equation (4.1) one can write

$$F_1 = k_{11}x_1 + k_{12}x_2$$

$$F_2 = k_{21}x_1 + k_{22}x_2$$

$$F_{12} = k_{12}x_2, \quad F_{22} = -k_2x_2 - k_{12}x_2$$

where  $F_{12}$  is the force on mass  $m_1$  due to displacement of mass  $m_2$  and  $F_{22}$  is the force on mass  $m_2$  due to displacement of mass  $m_2$ . Therefore;

$$k_{12} = k_{21} = -k, \quad k_{11} = k_1 + k, \quad k_{22} = k_2 + k$$

The eigenvalue equation of the coupled system without driving force and damping is:

$$[M^{-1}K - \omega^2 I] A = 0 \tag{4.3}$$

where  $A$  is some constant and  $\omega$  is an angular frequency. Assume that the system is sitting in a viscous fluid that gives a uniform damping  $\tau = \gamma I$ .

In a fullerene molecule, there are three times as many  $\sigma$  electrons as  $\pi$  electrons. For the mechanical model of a fullerene as shown in figure 22, we would assign the masses an electric charge of  $3q$  and  $q$  and subject the system to a periodic electric

field so that the force is given by

$$F(t) = \begin{bmatrix} 3 \\ 1 \end{bmatrix} f_0 \cos \omega t.$$

For a damped oscillator with a harmonic driving force one write the equation of motion;

$$\frac{d^2}{dt^2}X(t) + \Gamma \frac{d}{dt}X(t) + \omega_0^2 X(t) = F(t)/m$$

Accordingly, one can look for an irreducible, steady state solution to the equation of motion of the form

$$Z(t) = W e^{-i\omega t}$$

where  $W$  is a constant vector which yields the matrix equation

$$W = [M^{-1}K - \omega^2 I - i\gamma\omega I]^{-1} M^{-1}F_0$$

with

$$M^{-1}F_0 = \begin{bmatrix} \frac{3}{m_1+m_2} \\ \frac{1}{m_1+m_2} \end{bmatrix}$$

Now

$$M^{-1}K - \omega^2 I - i\gamma\omega I = \begin{bmatrix} \frac{k_1+k}{m_1} - \omega^2 - i\gamma\omega & \frac{-k}{m_1} \\ \frac{-k}{m_2} & \frac{k_2+k}{m_2} - \omega^2 - i\gamma\omega \end{bmatrix} \quad (4.4)$$

$$\text{or } \omega^2 - i\gamma\omega = \frac{1}{2} \left( \frac{k_1+k}{m_1} + \frac{k_2+k}{m_2} \right) \pm \sqrt{\frac{1}{4} \left( \frac{k_1+k}{m_1} - \frac{k_2+k}{m_2} \right)^2 + \frac{k^2}{m_1 m_2}} \quad (4.5)$$

If we represent the two roots of (4.5) by  $A$  and  $B$  as shown below, the product of  $A$  and  $B$  gives the determinant of matrix (4.4).

$$\begin{aligned}
 A &= \left[ \frac{1}{2} \left( \frac{k}{m_1} + \frac{k}{m_2} + \frac{k_1}{m_1} + \frac{k_2}{m_2} \right) \right. \\
 &\quad \left. + \sqrt{\frac{1}{4} \left( \frac{k}{m_1} - \frac{k}{m_2} + \frac{k_1}{m_1} - \frac{k_2}{m_2} \right)^2 + \frac{k^2}{m_1 m_2} - \omega^2 - i\gamma\omega} \right] \\
 B &= \left[ \frac{1}{2} \left( \frac{k}{m_1} + \frac{k}{m_2} + \frac{k_1}{m_1} + \frac{k_2}{m_2} \right) \right. \\
 &\quad \left. - \sqrt{\frac{1}{4} \left( \frac{k}{m_1} - \frac{k}{m_2} + \frac{k_1}{m_1} - \frac{k_2}{m_2} \right)^2 + \frac{k^2}{m_1 m_2} - \omega^2 - i\gamma\omega} \right]
 \end{aligned}$$

Then

$$[M^{-1}K - \omega^2 - i\gamma\omega]^{-1} = \frac{1}{A \cdot B} \times \begin{bmatrix} \frac{k_1+k}{m_1} - \omega^2 - i\gamma\omega & \frac{-k}{m_1} \\ \frac{-k}{m_2} & \frac{k_2+k}{m_2} - \omega^2 - i\gamma\omega \end{bmatrix} \quad (4.6)$$

If we then isolate the contributions of the two zeros in the denominator of (4.5)

we can write

$$[M^{-1}K - \omega^2 - i\gamma\omega]^{-1} = \frac{1}{2B} \begin{bmatrix} 1 & 1 \\ 1 & 1 \end{bmatrix} + \frac{1}{2A} \begin{bmatrix} 1 & -1 \\ -1 & 1 \end{bmatrix}$$

with

$A = a - i\gamma\omega$ , with

$$a = \left[ \frac{1}{2} \left( \frac{k}{m_1} + \frac{k}{m_2} + \frac{k_1}{m_1} + \frac{k_2}{m_2} \right) + \sqrt{\frac{1}{4} \left( \frac{k}{m_1} - \frac{k}{m_2} + \frac{k_1}{m_1} - \frac{k_2}{m_2} \right)^2 + \frac{k^2}{m_1 m_2} - \omega^2} \right]$$

$$B = b - i\gamma\omega, \text{ with}$$

$$b = \left[ \frac{1}{2} \left( \frac{k}{m_1} + \frac{k}{m_2} + \frac{k_1}{m_1} + \frac{k_2}{m_2} \right) - \sqrt{\frac{1}{4} \left( \frac{k}{m_1} - \frac{k}{m_2} + \frac{k_1}{m_1} - \frac{k_2}{m_2} \right)^2 + \frac{k^2}{m_1 m_2} - \omega^2 - i\gamma\omega} \right]$$

$$\begin{bmatrix} \alpha_1 + i\beta_1 \\ \alpha_2 + i\beta_2 \end{bmatrix} (\cos \omega t - i \sin \omega t) = \begin{bmatrix} \alpha_1 \cos \omega t + \beta_1 \sin \omega t \\ \alpha_2 \cos \omega t + \beta_2 \sin \omega t \end{bmatrix}$$

with

$$\alpha_1 = \left\{ \left( \frac{b}{b^2 + \gamma^2 \omega^2} \right) \left( \frac{3}{2m_1 + 2m_2} + \frac{1}{2m_1 + 2m_2} \right) + \left( \frac{a}{a^2 + \gamma^2 \omega^2} \right) \left( \frac{3}{2m_1 + 2m_2} - \frac{1}{2m_1 + 2m_2} \right) \right\} f_0$$

$$\alpha_2 = \left\{ \left( \frac{b}{b^2 + \gamma^2 \omega^2} \right) \left( \frac{3}{2m_1 + 2m_2} + \frac{1}{2m_1 + 2m_2} \right) - \left( \frac{a}{a^2 + \gamma^2 \omega^2} \right) \left( \frac{3}{2m_1 + 2m_2} - \frac{1}{2m_1 + 2m_2} \right) \right\} f_0$$

$$\beta_1 = \gamma\omega \left\{ \left( \frac{1}{b^2 + \gamma^2 \omega^2} \right) \left( \frac{3}{2m_1 + 2m_2} + \frac{1}{2m_1 + 2m_2} \right) + \left( \frac{1}{b^2 + \gamma^2 \omega^2} \right) \left( \frac{3}{2m_1 + 2m_2} - \frac{1}{2m_1 + 2m_2} \right) \right\} f_0$$

$$\beta_2 = \gamma\omega \left\{ \left( \frac{1}{b^2 + \gamma^2 \omega^2} \right) \left( \frac{3}{2m_1 + 2m_2} + \frac{1}{2m_1 + 2m_2} \right) - \left( \frac{1}{b^2 + \gamma^2 \omega^2} \right) \left( \frac{3}{2m_1 + 2m_2} - \frac{1}{2m_1 + 2m_2} \right) \right\} f_0$$

$$X(t) = \begin{pmatrix} \alpha_1 \cos \omega t + \beta_1 \sin \omega t \\ \alpha_2 \cos \omega t + \beta_2 \sin \omega t \end{pmatrix} \rightarrow \frac{dX(t)}{dt} = \begin{pmatrix} -\alpha_1 \omega \sin \omega t + \beta_1 \omega \cos \omega t \\ -\alpha_2 \omega \sin \omega t + \beta_2 \omega \cos \omega t \end{pmatrix}$$

$$F(t) = \begin{bmatrix} 3 \\ 1 \end{bmatrix} f_0 \cos \omega t \quad F(t)^T = \begin{pmatrix} 3 & 1 \end{pmatrix} f_0 \cos \omega t$$

The power expended by the external force is summed over all the degrees of freedom of the force times the velocity:

$$P = F(t)^T \frac{dX(t)}{dt}$$

$$P = [3, 1] \begin{bmatrix} -\alpha_1 \omega \sin \omega t + \beta_1 \omega \cos \omega t \\ -\alpha_2 \omega \sin \omega t + \beta_2 \omega \cos \omega t \end{bmatrix} f_0 \cos \omega t$$

The average power lost to the frictional force comes from the  $\cos^2 \omega t$  term

$$P = 3\beta_1 \omega f_0 + \beta_2 \omega f_0 \tag{4.7}$$

### 5.3.4 Result and discussion

The discovery of fullerene molecules by Smalley et al [5] as a third form of carbon (besides graphite and diamond) was quite surprise. Subsequent study of these amazing molecules was understandably intense and is still ongoing. One branch of this

research focusses on the possible use of fullerenes in electronics. Our group has been involved in the study of collective excitations of  $C_{60}$  applying a semiclassical method, the local current approximation, in conjunction with the equation of motion approach to find multipole oscillations [93]. In this analysis we realized that the main features of the treatment of such a complicated system can be well understood in terms of the simple mechanical model studied here. In particular, the interpretation of the different responses of  $\pi$ - and  $\sigma$ - electrons could thus be made more transparent. This has initially been a disputed interpretation of experimental results, although it has been widely accepted now.

We compare our results (figure 24) with the experimental work (figure 25). The first peak in each picture is due to the  $\pi$  electrons and the high energy peak is due to  $\sigma$  electrons. These two peaks are corresponding to the two frequencies  $\omega_1$  and  $\omega_2$  of low and high energy modes, the first peak being much more prominent.

Ju et al [67] from their theoretical and experimental electron energy loss spectroscopy (EELS) reported the low energy mode of  $C_{60}$  around 6 – 10 eV and high energy mode around 18 – 22 eV. In agreement with the experimental work we found a low energy mode approximately at 10 eV and high energy mode around 22 eV. Our computation meets the upper limit of the experimental work. These two modes are the analogues of the  $\pi$  and  $\sigma$  plasmons in graphite [95], [96] and the corresponding plasmons observed in solid  $C_{60}$  [11], [67] and references there in. While our simple mechanical model corroborate the distinction between  $\pi$  and  $\sigma$  electron responses, it can not mimick the volume plasmon effects observed at higher frequencies [14], [12],

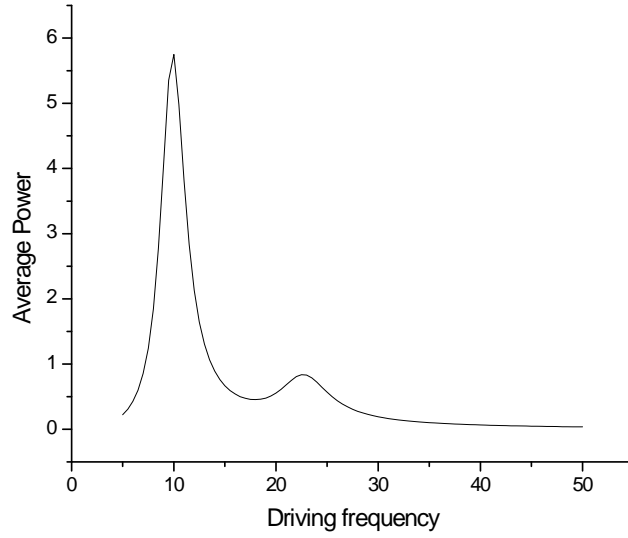


Figure 24: The average power lost by damped oscillator

[13], [61]. The shape of these two peaks depends on the stiffness of the springs and the frequency of the driving force. In this computation, the stiffness  $k$  of the spring coupling the two masses, is much less than those of the outer two springs. The frequency of each resonance peak depend on the coupling strength and damping terms as well. The two resonance peaks due to the oscillations of  $\pi$  and  $\sigma$  electrons are found at the frequencies:

$$\omega^2 - i\gamma\omega = \frac{1}{2} \left( \frac{k_1 + k}{m_1} + \frac{k_2 + k}{m_2} \right) - \sqrt{\frac{1}{4} \left( \frac{k_1 + k}{m_1} - \frac{k_2 + k}{m_2} \right)^2 + \frac{k^2}{m_1 m_2}} \quad (4.7)$$

and

$$\omega^2 - i\gamma\omega = \frac{1}{2} \left( \frac{k_1 + k}{m_1} + \frac{k_2 + k}{m_2} \right) + \sqrt{\frac{1}{4} \left( \frac{k_1 + k}{m_1} - \frac{k_2 + k}{m_2} \right)^2 + \frac{k^2}{m_1 m_2}} \quad (4.8)$$

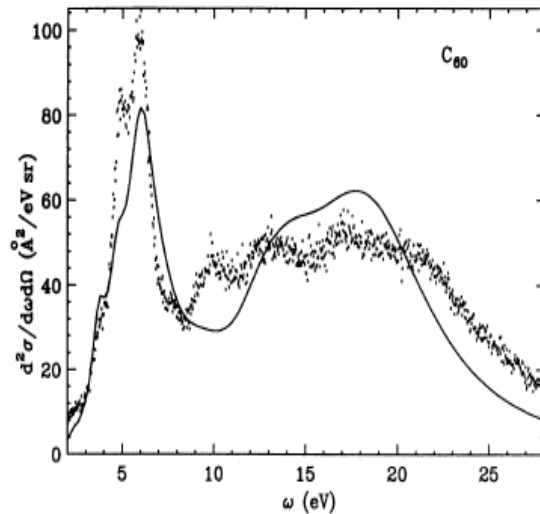


Figure 25: Inelastic electron excitation cross section of fullerene molecules, solid line (theoretical result) and points (experimental result),(used by permission of author)

We have shown how the two frequencies vary with the coupling strength. One arrives at the normal mode vectors of vibration by substituting these angular frequencies into the eigenvalue equation. From the comparison of these two plots one can conclude that the photoexcitation of fullerenes and power consumption of a classical oscillator system are of similar nature.

## 6 Presentations and Publications

During the period of this research work, I got an opportunity to participate in several conferences in and out of the USA. The following is a complete list of the conferences and our publications related to my work.

1. Annual meeting of the American Physical Society, California Section, October 27-28, 2006, California State University Long Beach, CA.

2. Annual meeting of the American Physical Society, California Section, October 26-27, 2007, Lawrence Berkeley National Laboratory, CA.

3. Progress in Electromagnetic Research Symposium (PIERS), Beijing, China, March 26-30, 2007.

4. Annual meeting of the American Physical Society, California Section, October 29-30, 2010, California Institute of Technology, Pasadena, CA.

5. K. Lamichhane and P. Winkler, The Use of the Virial Theorem and Sum-rules in Atomic Structure Calculations. (Published, PIERS Proceedings, 330-333, March 26-30, Beijing, China, 2007)

- 6.K. Lamichhane, B. Bach and P. Winkler, Similarity of Photoexcitation Cross-sections of Fullerenes and the Power Consumption of a Classical Oscillator System. (submitted to American Journal of Physics, 2010).

7. K. Lamichhane, M. Brack and P. Winkler, Energies of Higher Multipole Vibrations of Fullerenes in a Semi-Classical Approach. (accepted for publication, International Journal of Quantum Chemistry, 2010).

## References

- [1] Mie, Ann. Phys. (Leipzig) **25**, 376-445 (1908)
- [2] W. D. Knight, Keith Clemenger, W. A. de Heer, W. A. Saunders, M. Y. Chou and M. L. Cohen, Phys. Rev. B **31**, 2539 (1985)
- [3] M. Brack, Rev. Mod. Phys. **65**, 677 (1993)
- [4] S. Link and M. A. El-Sayed, Int. Rev. Phys. Chem. **19**, 409 (2000)
- [5] H. W. Kroto, J. R. Heath, S. C. O'Brien, R. F. Curl and R. E. Smalley, Nature **318** (1985) 162.
- [6] E. A. Rohlfing, D. M. Cox and A. Kaldor, J. Chem. Phys. **81**, 3322-3330, (1984)
- [7] R. Taylor, *The chemistry of fullerene*, Adv. series in fullerene, vol **4**, World Scientific Publishing Co. Pte. Ltd, Singapore,1995
- [8] R. A. Phaneuf, *Handbook of nanophysics* edited by Klaus D. Satter, Vol. **2**, September 7th 2010.
- [9] S. Satpathy, Chem. Phys. Lett. **130**, 545 (1986)
- [10] S. Saito and A. Oshiyama, Phys. Rev. Lett. **66**, 2637 (1991)
- [11] J. H. Weaver, Jose Luis Martins, T. Komeda, Y. Chen, T. R. Ohno, G. H. Kroll, N. Troullier, R.E. Haufler and R. E. Smalley, Phys. Rev. Lett. **66**, 1741 (1991)

- [12] G. F. Bertsch, A. Bulgac, D. Tomanek, Y. Wang, Phys. Rev. Lett. **67**, 2690 (1991)
- [13] I. V. Hertel, H. Steger, J. de Vries, B. Weisser, C. Menzel, B. Kamke and W. Kamke, Phys. Rev. Lett. **68**, 784 (1992)
- [14] S. W. J. Scully, E. D. Emmons, M. F. Gharaibeh, R. A. Phaneuf, A. L. D. Kilcoyne, A. S. Schlachter, S. Schippers, A. Müller, H. S. Chakraborty, M. E. Madjet and J. M. Rost, Phys. Rev. Letters, **94**, 065503 (2005) .
- [15] E. Lipparini et al, Phys. Rev. Lett. Vol. **36**, No. 12 (1976)
- [16] J. Martorell et al, Phys. Lett. Vol. **60B**, No. 4 (1976)
- [17] K. Goeke and J. Speth, Nuc. Phys. A2. **96**, 109-133 (1978)
- [18] L. J. Tassie, Australian J. Phys. **11** 481 (1958)
- [19] J. P. Elliott, *Collective Motion in Nuclei*, September 17 (1958)
- [20] M. Goldhaber and E. Teller, Phys. Rev, Vol **74**, 1046,(1948)
- [21] H. von Steinwedel and J. H. D. Jensen, Z. Naturf. Teil A **5**, 413 (1950).
- [22] W. D. Myers, W. J. Swiatecki, T. Kodama, L. J. El-Jaickand E. R. Hilf, Physical Review C, Vol **15**, 2032, (1977)
- [23] *Giant multipole resonances* edited by Fred E. Bertrand, Harwood Academic Publishers, New York (1979).

- [24] J. Speth, Nuc. Sci. Research Conference Series Vol. **1** (1980)
- [25] G. F. Bertsch and R. A. Broglia, *Oscillation in finite quantum system*, Cambridge University Press, UK (1994).
- [26] W. Kohn and L. J. Sham, Physical Review, Vol **140**, A1133, (1965)
- [27] P. Hohenberg and W. Kohn, Physical Review, Vol **136**, B864, 9 November, 1964
- [28] J. M. Thijssen, *Computational Physics*, Cambridge University Press, (1999).
- [29] W. Ekardt, Physics Review Letters, Vol **52**, 1925, (1984)
- [30] W. Ekardt and Z. Penzar, Physical Review B, Vol **43**, 1322, 1991-I
- [31] R. O. Jones, NIC Series, Vol. **31**, ISBN 3-00-017350-1, PP 45-70 (2006)
- [32] G. Vinagle, W. Kohn, Physical Review Letters, Vol **77**, 2037 (1996)
- [33] G. Vinagle, C. A. Ullrich, S. Conti, Phys. Rev. Letters, Vol **79**, 4878 (1997)
- [34] M. Brack and R. K. Bhaduri: *Semiclassical Physics*, Westview Press, Colorado, 2003
- [35] R. O. Jones and O. Gunnarsson, *The density functional formalism, its applications and prospects*, Rev. Mod. Phys. **61**, 689, (1989)
- [36] S. Kümmel and M. Brack, Phys. Rev A, Feb 2, 2008
- [37] M. Brack, Physical Review B, Vol **39**, 3533, 1989-II

- [38] D. J. Thouless, Nucl. Phys. A **22**, 78 (1961)
- [39] J. Simons and W. D. Smith, J. Chem. Phys., **58**, 4899-4907 (1973)
- [40] E. Anderson and J. Simons, J. Chem. Phys., **65**, 5393-97 (1976)
- [41] C. W. McCurdy, T. N. Rescigno, D. I. Yeager and V. Mckoy, in " Modern Theoretical Chemistry, Vol. **3**, pp 339-86 (1977), New York, Plenum
- [42] R. J. Bartlett, Int. J. Mol. Sci. **3**, 579-603 (2002)
- [43] J. F. Stanton and J. Gauss, Adv. Chem. Phys. **125**, 101-46 (2003)
- [44] A. I. Krylov, "Equation-of-Motion Coupled -Cluster Methods for Open-Shell and Electronically Excited Species: The Hitchhiker's Guide to Fock Space", Annu. Rev. Phys. Chem. **59**, 433-62 (2008)
- [45] S. Kümmel, Ph. D. Thesis, Regensburg University: *Structure and optical properties of sodium clusters studied in density functional theory* (Logos, Berlin, 2000)
- [46] see, e.g., D. J. Rowe, *Nuclear collective motion* (Methuen, London, 1970)
- [47] S. Wang, Phys. Rev. A **60**, 262 (1999)
- [48] *Theory and application of moment methods in many-fermion systems* edited by B. J. Dalton, S.M. Grimes, J. P. Vary, S.A. Williams, page 463-499, Plenum Press, New York, (1979)
- [49] O. Bohigas, A. M. Lane, J. Martorell, Physics Reports **51**, No. 5 (1979) 267-316

- [50] Joachim Alexander Maruhn and Paul-Gerhard Reinhard, *Simple models of many fermion systems*, Springer, New York, 2010
- [51] A. A. Kamzolov, Communication of the Moscow Mathematical society, Bernstein's inequality for fractional derivatives of polynomials in spherical harmonics, (1982).
- [52] A. B. Migdal, J. Phys. USSR **8**, 331 (1944)
- [53] See, e.g., the review by B.K. Jennings and A.D. Jackson, Phys. Rep. **66**, 141 (1980)
- [54] G. F. Bertsch and W. Ekardt, Phys. Rev. B **32**, 7659 (1985)
- [55] W. A. de Heer, Rev. Mod. Phys. **65**, 611 (1993)
- [56] P.-G. Reinhard, M. Brack, O. Genzken, Phys. Rev. A **41**, 5568 (1990)
- [57] S. Kümmel, M. Brack, P.-G. Reinhard, Phys. Rev. B **58**, R1774 (1998)
- [58] C. J. Powell and J. B. Swan, Phys. Rev. **115**, 869-875 (1959)
- [59] See, for example, C. Kittel, *Introduction to solid state physics*, Wiley, New York, (1996); pp. 276-278
- [60] M. J. Puska and R.M. Nieminen, Phys. Rev. A **47**, 1181 (1993)
- [61] M. Brack, P. Winkler, M. V. N. Murthy, Int.J. Mod. Phys. Vol. **17**, 138, Feb, (2008)
- [62] M. Schmidt and H. Haberland, Eur. Phys. J. D **6**, 109-118 (1999)

- [63] A. Rüdél, R. Hentges, U. Becker, H. S. Chakraborty, M. E. Madjet, and M. Rost, Phys. Rev. Lett. **89**, 125503 (2002)
- [64] A. V. Korol and A.V. Solov'yov, Phys. Rev. Lett. **98**, 179601 (2007)
- [65] S. W. J. Scully, E. D. Emmons, M. F. Gharaibeh, R. A. Phaneuf, A. L. D. Kilcoyne, A. S. Schlachter, S. Schippers, A. Müller, H. S. Chakraborty, M. E. Madjet and J. M. Rost, Phys. Rev. Lett. **89**, 179602 (2007)
- [66] G. F. Bertsch, A. Bulgac, D. Tomanek, and Y. Wang, Phys. Rev. Lett. **67**, 2690-2693 (1991)
- [67] N. Ju, A. Bulgac and J. W. Keller, Physical Review B, Vol **48**, 9071, 1993-II
- [68] L. G. Gerchikov, Andrey N Ipatov, Andrey V Solov'yov and Walter Greiner, J. Phys. B: At. Mol. Opt. Phys. **31**, 3065-3077, (1998)
- [69] O. Frank and J. M. Rost, Phys. Rev. A **60**, 392 (1998)
- [70] O. Frank and J. M. Rost, Chem. Phys. Lett. **271** (1997) 367-371
- [71] S. Keller et al, J. Phys. B: At. Mol. Opt. Phys. **30** (1997)
- [72] Th. Hirschmann, M. Brack, and P.-G. Reinhard, Z. Phys. D **40**, 254-257 (1997)
- [73] John W. Keller and M.A. Coplan, Chem. Phys. Lett, Vol. **193**, 89 (1992)
- [74] G. Barton and C. Eberlein, J. Chem. Phys. **95** (3), (1991)
- [75] C. Xia, C. Yin and V. V. Kresin, Phys. Rev. Letters, **17** 183-185, (2009)

- [76] Katja Hollich, Ulrich Gosele, and Silke Christianen, Phys. Rev. Letters, **103**, 087404 (2009)
- [77] A. Gagen and S. Larson, <http://online.redwoods.cc.ca.us/instruct/dornald/deproj/spoo/seanal> (2000)
- [78] R. G. Polozkov, V. K. Ivanov, and A. V. Solov'yov, J. Phys. B: At. Mol. Opt. Phys. **38** (2005) 4341-4348
- [79] Iain G. Main, *Vibrations and waves in physics*, Cambridge University Press, (1990)
- [80] Howard Georgi, *The physics of waves*, Harvard University, Prentice Hall, (1993)
- [81] P. -G. Reinhard, M. Brack and O. Genzken, Phys. Rev. A, Vol. **41**, 5568, (1990)
- [82] M. Brack, reviews of modern physics, Vol. **65**, 677, 1993
- [83] A. Bulgac and N. Ju, Phys. Rev B, **46**, 4297, 1992-I
- [84] W. Kohn, Phys. Rev A, Vol **34**, 737, 1986
- [85] S. Kümmel, M. Brack, and P-G. Reinhard, Phys. Rev. B **58**, R1774 (1998)
- [86] M. Madjet, C. Guet and W. R. Johnson, Phys. Rev A, Vol **51**, 1327, 1995
- [87] M. L. Perlman and G. Friedlander, Phys. Rev **74**, 442 (1948).
- [88] P. Gleissl, M. Brack, J. Meyer, and P. Quentin, Ann. Phys. (N.Y.) 197, 205-264 (1990)

- [89] S. Lundqvist and N. March, *Theory of inhomogeneous electron gas*, plenum, New York, 1983
- [90] P. Phariseau and W. M. Temmerman, *The electronic structure of complex system*. NATO ASI series B, Plenum, New York, 1984
- [91] V. K. Ivanov G. Yu. Kashenok, R. G. Polozkov and A. V. Solov'yov, J. Expt. and Theor. Phys. Vol. **96**, 658-668, 2003
- [92] M. A. L Marques and E. K. U. Gross, Annu. Rev. Phys. Chem. 2004, 55:427-55
- [93] K. Lamichhane, M. Brack and P. Winkler, Energies of higher multipole vibrations of fullerenes in a semi-classical approach, to be appeared in International Journal of Quantum Chemistry
- [94] J. L. Martin, N. Troullier, and J. H. Weaver, Chem. Phys. Lett. **180**, 457 (1991)
- [95] K. Zeppenfeld, Z. Phys. **243**, 229 (1971)
- [96] H. H. Venghaus, Phys. Status Solidi B **71**, 609 (1975)